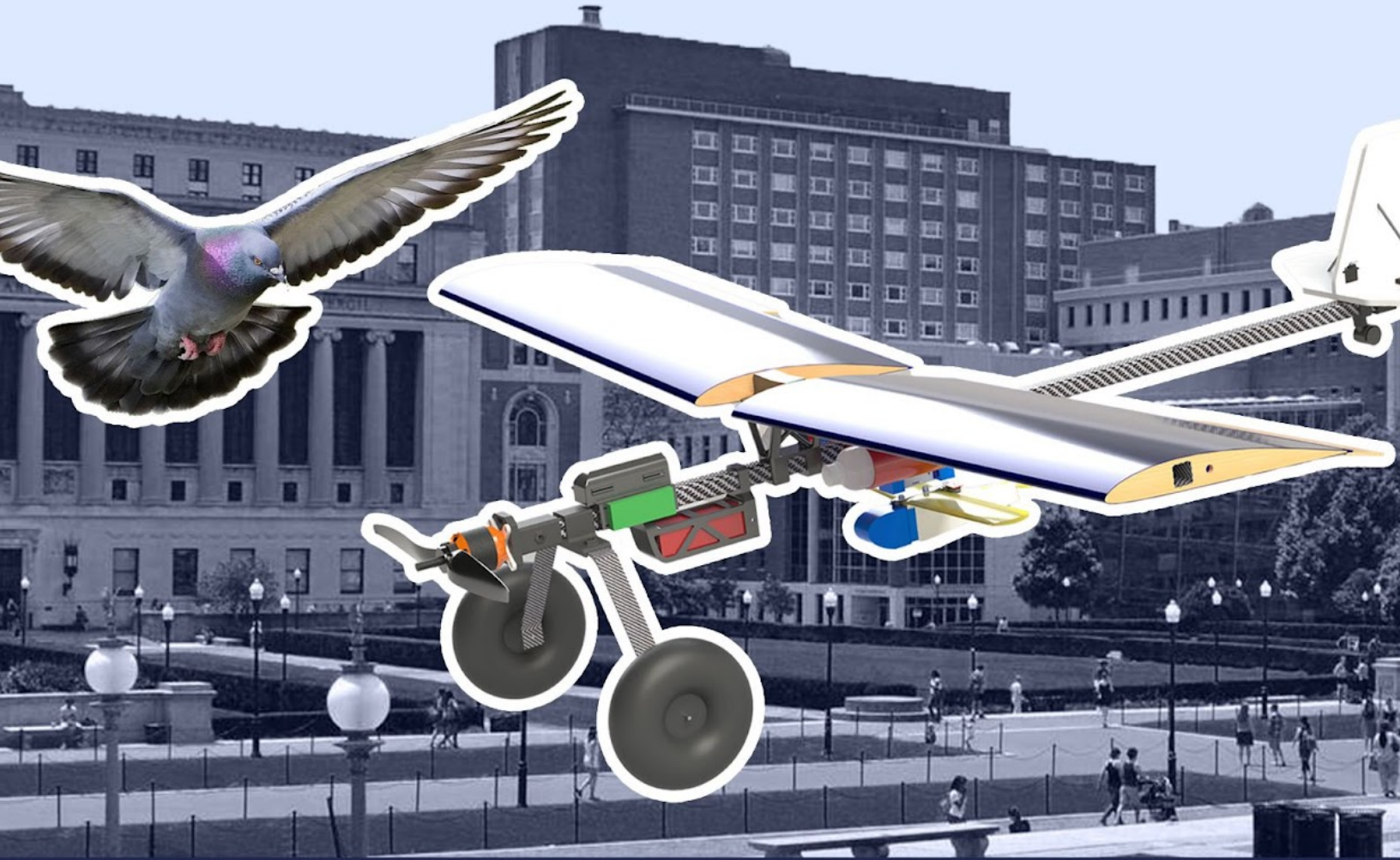


CARRIER PIGEON



COLUMBIA UNIVERSITY IN THE CITY OF NEW YORK



AIAA DESIGN/BUILD/FLY
2024-25 DESIGN REPORT



Table of Contents

I. Nomenclature/Acronyms	3
1. Executive Summary	4
2. Management Summary	5
2.1. Team Organization	5
2.2. Milestone Chart	6
3. Conceptual Design	6
3.1. Mission Requirements	7
3.2. Translation to Design Requirements	8
3.3. Score Sensitivity Analysis	10
3.4. Configuration Selection	11
3.5. Final Conceptual Design Configuration	16
4. Preliminary Design	17
4.1. Design and Analysis Methodology	17
4.2. Design and Sizing Trade Studies	17
4.3. Performance Prediction Methodology	21
4.4. Aerodynamics and Stability Prediction	22
4.5. Mission Performance Estimation	26
5. Detailed Design	27
5.1. Dimensional Parameters of the Final Design	27
5.2. Structural Characteristics and Capabilities	28
5.3. Subsystem Design	28
5.4. Propulsion and Avionics Characteristics	34
5.5. Weight and Balance	36
5.6. Predicted Flight and Mission Performance	37
5.7. Drawing Package	37
6. Manufacturing Plan	42
6.1. Investigated Processes, Selection Process, and Results	42
6.2. Detailed Manufacturing Processes	44
6.3. Manufacturing Milestone Chart	47
7. Testing Plan	48
7.1. Test Objectives and Schedule	48
7.2. Checklists	51
8. Performance Results	53
8.1. Ground Test Results	53
8.2. Flight Test Results	56
8.3. Differences to Predictions and Improvements	56
9. Bibliography	57



I. Nomenclature/Acronyms

2D	Two-Dimensional	FEA	Finite Element Analysis
3D	Three-Dimensional	FoM	Figure of Merit
AoA	Angle of Attack	FOS	Factor of Safety
ABS	Acrylonitrile butadiene	GM	Ground Mission
AIAA	American Institute of Aeronautics and Astronautics	GPS	Global Positioning System
AR	Aspect Ratio	IMU	Inertial Measurement Unit
CAD	Computer Aided Design	LASER	Light Amplification by Stimulated Emission of Radiation
CFD	Computational Fluid Dynamics	LiPo	Lithium Polymer
CG	Center of Gravity	M1	Mission 1
C_L	Coefficient of Lift	M2	Mission 2
C_D	Coefficient of Drag	M3	Mission 3
CNC	Computer Numerical Control	PLA	Polylactic Acid
CU	Columbia University	RC	Radio Controlled
DBF	Design, Build, Fly	Re	Reynolds Number
DC	Direct Current	RPM	Rotations Per Minute
ESC	Electronic Speed Controller	SLA	Stereolithography
FAA	Federal Aviation Administration	SLS	Selective Laser Sintering
Fig.	Figure	XTV	X-1 Test Vehicle
FDM	Fused Deposition Modeling		



1. Executive Summary

This report presents the Columbia University (CU) team's process of designing, manufacturing, and testing the radio-controlled (RC) aircraft *Carrier Pigeon* for the 2024-2025 American Institute of Aeronautics and Astronautics (AIAA) Design/Build/Fly (DBF) competition. CU designed the aircraft to perform four X-1 Supersonic Flight Program missions. In Mission 1 (M1), the aircraft completes a three lap delivery flight to demonstrate operational capabilities. In Mission 2 (M2), it carries the X-1 Test Vehicle (XTV) and fuel tanks in a captive carry flight with the aim to maximize fuel tank weight. In Mission 3 (M3), the aircraft completes a launch flight where it releases the XTV to be dropped in a specified zone. The ground mission (GM) requires the team to rapidly transition configurations for each of the three flight phases, including XTV release.

Carrier Pigeon is a single-engine RC aircraft in a dihedral constant chord high-wing configuration. The main wings feature a Selig S7055 flat-bottomed airfoil for improved lift characteristics. A conventional tail ensures stable flight and effective pitch control. *Carrier Pigeon* is powered by a 22.2 V, 99.9 Wh Lithium Polymer (LiPo) battery, and its propulsion system features a 16x6E propeller mounted to a single Avian 5065-450 Kv, 1200 W motor. The propulsion system enables a thrust-to-weight ratio of around 2, yielding a predicted maximum cruise speed of 66 ft/s. Mission-specific spring-loaded bottle mounts and a mechanical drop mechanism were designed to quickly secure the fuel tanks and XTV, without disrupting the aircraft's aerodynamics, weight distribution, or GM assembly/disassembly. After the test campaign, adjustments, and flight performance tests, the predicted performance table values were found and validated.

Carrier Pigeon was designed by 30 students studying diverse disciplines across engineering, physics, and computer science who worked in four subteams (Aerodynamics, Structures, Electrical/Propulsion, and Payloads) based on strengths, experience, and interests. Planning was subdivided into three phases, conceptual, preliminary and detailed design. Competition constraints guided the initial aircraft's configuration, and the configuration was refined by iterating through sensitivity studies, off-site flight tests, and Finite Element Analysis (FEA). For the preliminary design, the team determined wing and empennage dimensions, and propulsion system components based on constraint analysis and performance trade studies. This dictated improvements and following prototype manufacturing which was comparatively streamlined due to the lack of a fuselage. This allowed the team to focus on optimizing the propulsion system, materials, structure, and mission-specific component choices. The detailed design finalized these aspects, and formally encapsulated everything in the drawing package.

Table 1: *Carrier Pigeon* Performance Capabilities

Specifications	Value
Standing Weight	4.12 lb
Dry Weight (Includes Battery)	5.64 lb
Max Takeoff Weight	17.0 lb
Max Cruise Speed	66 ft/s
Fuel Tank + Adaptor Weight	4.36 lb
XTV Weight	0.49 lb
Ground Mission Time	45 s



Figure 1: Carrier Pigeon Render



2. Management Summary

2.1. Team Organization

The Columbia AIAA team consists of 30 undergraduate team members, including 2 seniors. The team is student-led and divided into an executive board and technical subteam roles, as shown in Fig. 2.

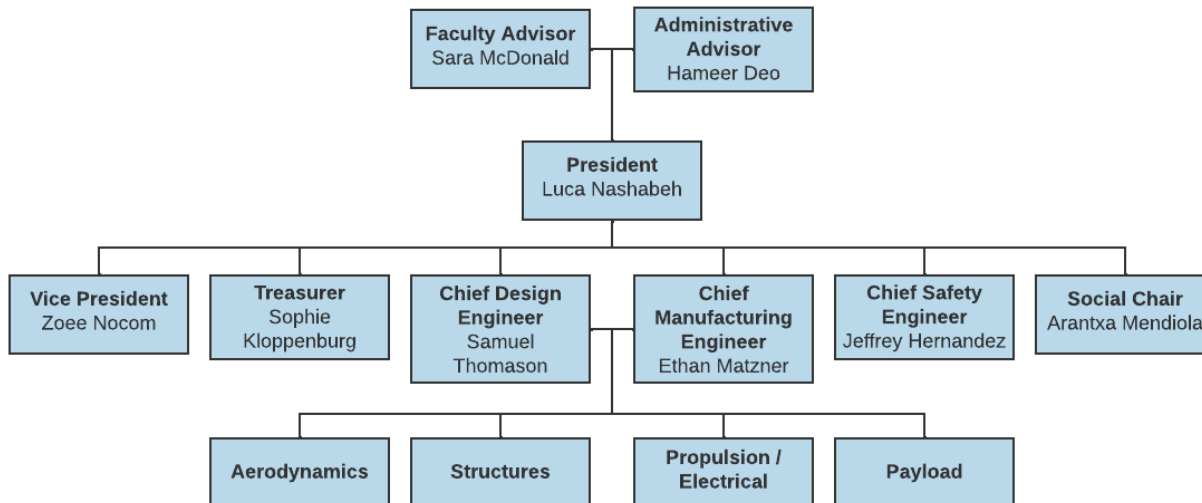


Figure 2: CU AIAA Organizational Chart

The president communicates with the university administration and oversees general planning. The vice president assists the president with administrative tasks and handles team-wide communications. The treasurer handles club finances, material purchases, and sponsorships. The chief design engineer directs the design and Computer Aided Design (CAD) process, with the chief manufacturing engineer directing the manufacturing and testing processes. The chief safety engineer ensures club activities adhere to lab conduct and safety guidelines. The social chair manages social media and organizes team events to foster community. The faculty and administrative advisors work to help with logistical challenges, providing, for example, technical advice and guidance for team budgeting.

The chief engineers guide four subteams: Aerodynamics, Structures, Propulsion/Electrical, and Payload. Each is led by a non-board member selected by the executive board on the basis of commitment and capability. Subteam leads serve as advisors for their respective subteams, ensure that deadlines are met, and mentor other team members for relevant skills and knowledge.

The Aerodynamics subteam designs the wings and empennage to optimize for flight stability and control, and conducts Computational Fluid Dynamics (CFD) analyses of the aircraft. The Propulsion/Electrical subteam selects and implements the battery, motor, propeller, Electronic Speed Controller (ESC), and other electrical systems. The Structures subteam designs the structural components of the aircraft (e.g. landing gear mount, motor mount, wing mount) using SOLIDWORKS, and conducts FEA to ensure structural integrity. The Payloads subteam, specific to this year, is responsible for the design and construction of the XTV and fuel tank pylons. While members are assigned a primary subteam, they are welcome to assist other subteams, allowing them to learn new skills and increase the team's overall productivity.



2.2. *Milestone Chart*

At the start of the academic year, the team created a Gantt chart to keep track of progress and establish a timeline for completing the aircraft. Each week, “Actual Progress” was updated according to club activities. Fig. 3 displays the aircraft’s progress at the time of writing this report alongside the proposed timeline.

Columbia DBF 2024-2025 🦁	September 2024				October 2024				November 2024				December 2024				January 2025				February 2025				March 2025				April 2025					
	9	16	23	30	7	14	21	28	4	11	18	25	2	9	16	23	30	6	13	20	27	3	10	17	24	3	10	17	24	31	7	14	21	28
Design																																		
Aero/Electrical/CAD Lessons																																		
Sensitivity Analysis					//////																													
Conceptual Design					//////																													
CAD of Prototype					//////																													
Design Adjustments					//////																													
CAD of Competition Aircraft										//////																								
Competition Aircraft Design Freeze					的竞争设计冻结于 02/17/25 😊																													
Manufacturing																																		
Part & Material Procurement					//////				//////																									
XTV Prototype									//////														//////											
Prototype Aircraft									//////																									
Competition Aircraft & XTV									//////														//////											
Testing																																		
Electrical Testing									//////													//////												
Propulsion Testing									//////																									
Structural Validation									//////													//////												
Fuel Tank Validation																						//////												
Glider Mechanism Testing																						//////												
Ground Testing																						//////												
Prototype Aircraft Test Flights																						2/9/25 😊												
Competition Aircraft Test Flight																						2/9/25 😊												
Administrative and Logistics																																		
Competition Rule Review					//////																													
Proposal									//////					10/31/24 😊																				
Design Report																						02/21/25 😊												
AIAA DBF Competition 2025																						04/10 - 04/13 😊												

Figure 3: CU AIAA 2024-2025 Milestone Chart

3. Conceptual Design

The AIAA DBF 2025 Competition challenges teams to design, build, and fly an aircraft simulating an X-1 Supersonic Flight Test Program, including launching an XTV [1]. The test program consists of four missions (one ground mission and three flight missions): demonstration of flight capabilities, transporting fuel in removable, external tanks, remotely launching the XTV, and an additional ground mission focused on rapid assembly and configuration changes.

During the conceptual design stage, the team prioritized flyability to ensure the successful completion of the missions outlined in the competition rules. Based on past experience, creating a stable aircraft was the most important factor in allowing controlled flight with varying payloads. The team has faced challenges in completing missions in prior years, so it was important to allow for a slightly larger margin of error in each mission instead of attempting to maximize point gain and risking a loss of control. The best way to verify flight characteristics is through a physical flight test, so it was important to get a prototype in the air early in the school year. As a result, taking an iterative approach to the conceptual design of the aircraft with an emphasis on control appeared to be the best path toward a successful aircraft for this year's competition.



3.1. Mission Requirements

The setup and requirements of each mission are briefly summarized below. The flight map used in all three flight missions is shown in Fig. 4.

3.1.1. Mission 1 – Delivery Flight

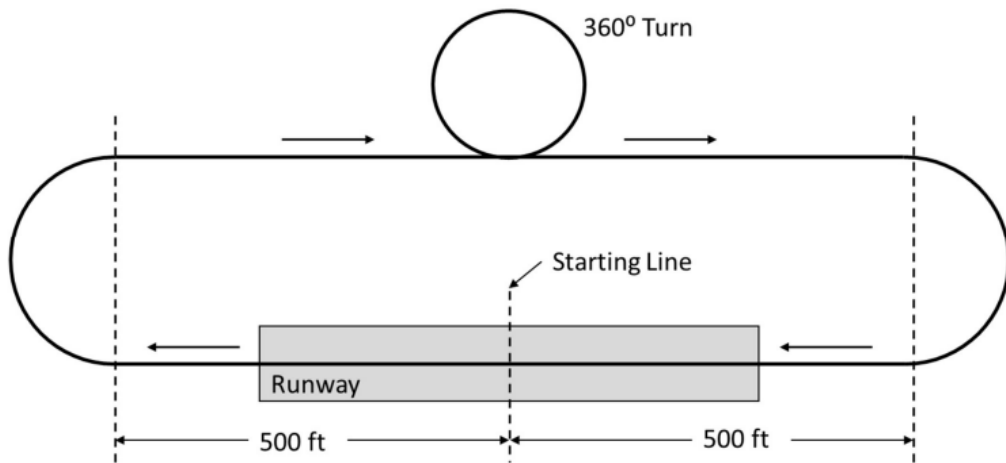


Figure 4: Nominal Flight Course

There is no payload for this mission. The aircraft will enter the staging box without the battery. During the five-minute staging window, the aircraft will be configured for flight, and the battery installed. It will then take off and fly three laps around the test track within a five-minute window before landing, with the landing not being included in the time. A lap is counted when the aircraft flies over the start/finish line in the air. A successful landing must be achieved to receive a score. A score of 1.0 is given for a successful mission.

3.1.2. Mission 2 – Captive Carry Flight

The payload for this flight is the XTV and fuel tanks. A minimum of two external fuel tanks must be used. The aircraft will enter the staging area with the payload and batteries removed, and all payload components will be installed within the five-minute staging window. The aircraft must fly three laps within a 5-minute window, and the score will be a function of the fuel weight and the time to fly three laps. The time starts when the aircraft begins to throttle up for the first takeoff, and a lap is considered complete when the aircraft passes over the start/finish line in the air. A successful landing must be completed to receive a score. Scoring for this mission is as follows:

$$M2 = 1 + \frac{N_{fuel\ weight} / \text{time to fly 3 laps}}{\max_{teams} (N_{fuel\ weight} / \text{time to fly 3 laps})}$$

3.1.3. Mission 3 – Launch Flight

The payload for this mission is the XTV and fuel tanks. External fuel tanks may be empty for this flight. The aircraft will be brought to the staging box and readied for flight as in M2. The mission will have a 5-minute flight window, and the scoring will be a function of the number of laps flown within that time. Additionally, the XTV may be released in flight, allowing for a number of bonus points if the test vehicle successfully executes a 180° turn, followed by a descending pattern or orbit before landing, and coming



to a stop in one of three designated bonus boxes adjacent to the runway. The XTV must also have flashing lights or strobes that activate after its release and should remain functional after landing. The aircraft must land successfully to receive a score. The score will be determined as follows:

$$M3 = 2 + \frac{N_{laps} + Bonus/W_{XTV}}{\max_{teams}(N_{laps} + Bonus/W_{XTV})}$$

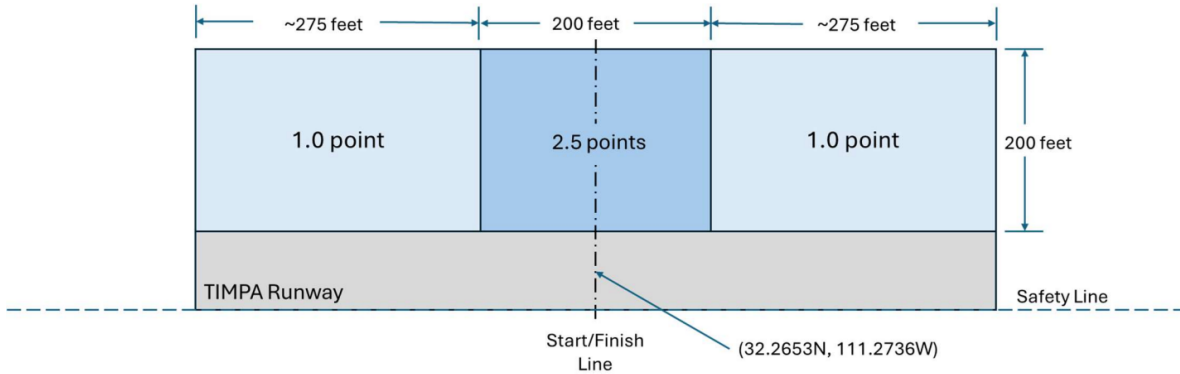


Figure 5: Bonus Point Scoring Boxes

3.1.4. Ground Mission – Configuration Demonstration

The ground mission is designed to measure the amount of time required to convert the aircraft from the fleet bomber configuration to the test configuration, and install all pylons and fuel tanks. Additionally, a successful separation of the XTV is demonstrated during this period. A designated ground crew member will assemble the aircraft and is the only person allowed to touch the aircraft and payloads, while a pilot verifies flight controls.

The mission will start with the aircraft on its landing gear, without the external fuel tank pylons, fuel tanks, or the XTV installed. The installation of the external pylons, fuel tanks, and the XTV are timed individually, and then verified by the ground mission judge, who will check that the components are secure and properly installed. The pilot will then verify all flight controls function properly, and release the XTV from the aircraft. The ground mission judge will verify the XTV lights turn on after release, and record the total mission time. The mission score is the function of the minimum mission time across all competitors divided by the team's specific mission time:

$$GM = \frac{\min_{teams}(time)}{time}$$

3.2. Translation to Design Requirements

From these mission setups and the 2024-25 AIAA DBF rules, a list of constraints and requirements were constructed, and are shown in Table 2. These were used to determine subsystem design requirements.



Table 2: Mission Requirements and Constraints

Category	Label	Requirement
General Requirements	GR.1	The aircraft must be remotely controlled
	GR.2	The wingspan cannot exceed 6 ft
	GR.3	The aircraft must be assembled within 5 minutes before each mission
	GR.4	The fuel tanks must have a minimum capacity of 16 fl oz
	GR.5	All external fuel tanks must attach to the aircraft using removable pylons
	GR.6	The XTV must be a glider capable of autonomous flight (no RC receivers)
	GR.7	The XTV must have flashing lights that turn on after release from the aircraft
	GR.8	The XTV must be capable of commanded release from the aircraft via the pilot's transmitter
	GR.9	The aircraft must complete a successful landing after each mission to receive a score
	GR.10	The propulsion system and radio control system must have an externally accessible arming plug and switch, respectively
	GR.11	The propulsion battery must not exceed 100 W-hr of stored energy
	GR.12	Maximum of one battery connected to each propulsion system
Mission 1	M1.1	Stage the aircraft for M1 (no fuel tank pylons)
	M1.2	Carry no payload
	M1.3	Fly 3 laps within 5 minutes
Mission 2	M2.1	Stage the aircraft for M2 (fuel tank pylons installed)
	M2.2	Carry XTV and filled fuel tanks
	M2.3	Fly 3 laps within 5 minutes
	M2.4	Maximize fuel tank weight, minimize time to fly 3 laps
Mission 3	M3.1	Stage the aircraft for M3 (fuel tank pylons installed)
	M3.2	Carry XTV and empty fuel tanks
	M3.3	Launch the XTV from 200-400 ft above ground level (AGL)
	M3.4	The XTV must make a 180-degree turn and land in the designated area within the 5-minute window (for bonus points)
	M3.5	Maximize number of laps flown in 5 minutes, minimize XTV weight
Ground Mission	GM.1	Starting with the aircraft with no payload installed, install the external pylons, then install the fuel tanks and XTV
	GM.2	Release the XTV from the aircraft with activated flashing lights
	GM.3	Minimize aircraft configuration time

The list of subsystem design requirements determined from Table 2 is shown in Table 3. The mission requirement from which each subsystem requirement was derived is listed in Table 3.



Table 3: Subsystem Design Requirements

Category	Label	Mission Requirement	Subsystem Requirement
Aerodynamics	A.1	M2.3, M3.5	Minimize drag to minimize propulsion energy required and maximize speed
	A.2	M2.4	Maximize lift to carry more payload
Propulsion / Electrical	E.1	M1.3, M2.3, M3.5	The propulsion system must provide sufficient thrust to overcome drag in all flight configurations
	E.2	M3.5	The propulsion system must have at least 5 minutes of endurance while maintaining optimal M3 flight speed
	E.3	GR.10	The propulsion system and radio control system must be easy to disable
Structures	S.1	M2.2, M3.2	All structural components must be able to withstand maximum load cases in all flight regimes
	S.2	M1.2, M2.2, M3.2	Ensure the plane remains stable under various loading configurations
Payload	P.1	GR.3, GR.5, GM.3	Removable pylons and XTV must be quick to install to configure the payloads in minimum time
	P.2	GR.8, M3.3, GM.2	Implement solenoid release mechanism for XTV release
	P.3	M3.4	Implement GPS to aid the XTV in landing within the designated zone
	P.4	GR.7, GM.2	Implement Hall Effect sensor circuit to turn on flashing lights after XTV release

3.3. Score Sensitivity Analysis

Using the scoring criteria detailed in Section 3.1, a sensitivity analysis study was performed using Python to determine what factors would maximize the total score. This sensitivity analysis assumes that all missions are completed successfully and that the aircraft flies in near ideal conditions; the validity of these assumptions are discussed further below. With these assumptions, a simplified but physically motivated model for the aircraft's performance was constructed, examining parameters such as motor power, battery capacity, payload mass for M2, maximum acceleration, and GM completion time.

To give more detail, the operating power was used to estimate a cruise velocity given a quadratic drag force. This cruise velocity is used for the straight portions of flight. Maximum turning acceleration, on the other hand, is used to estimate an optimal turn radius and velocity for the different in-flight maneuvers. Finally, total mass is used to estimate a takeoff time given the takeoff configuration and operation. The results from this simplified model are summarized in Fig. 6 and 7 below.

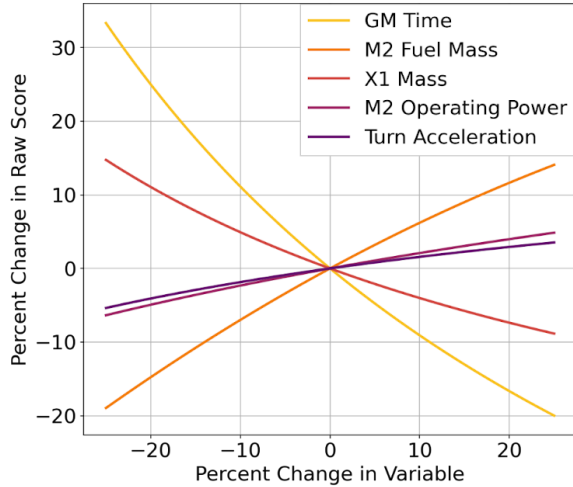


Figure 6. Sensitivity of raw mission scores.
Parameters are ordered by importance

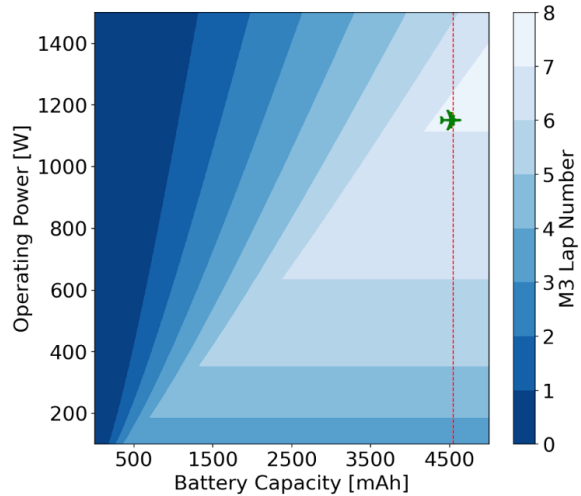


Figure 7. Propulsion system optimization for M3.
Red line indicates maximum propulsion system energy.

For M2, the fuel weight is both the most critical parameter—as it directly impacts the mission score—and the easiest to optimize. For M3, the mass of the XTV impacts the total score with roughly as much weight. The GM presents both the largest scoring weight while also being straightforward to optimize.

Thus, based on this sensitivity analysis, the GM optimization was prioritized—via the speed of the fuel tank and XTV attachment systems—then M2 fuel weight and M3 XTV mass, and finally the propulsion system. To choose optimal parameters for the propulsion system, a sensitivity study for M3 flight was performed. Fig. 7 shows that a 22.2 V, 4500 mAh battery (99.9 Wh) and 1150 W operating power provide the maximum number of M3 laps while complying with competition rules.

More fundamentally, and not captured by the above continuous analysis, is that completing a mission is required to score any points. In particular, the assumptions that all flights are completed successfully and in ideal conditions are not realistic. As such, stability, control authority, and consistency are important for the final conceptual design. These qualities cannot easily be captured in the continuous sensitivity analysis since they primarily contribute in a binary and stochastic manner, so it is difficult to quantify the extent to which these qualities should be emphasized in the conceptual design. Given experience in previous competitions however—and that a minimum of 4 out of 7 points are available for completion of all flight missions—these factors are strongly emphasized.

3.4. Configuration Selection

The optimal aircraft configuration was determined with each major subsystem being analyzed using relevant Factors of Merit (FoM). Table 4 outlines the process used to reach the ideal configuration decision.



Table 4: Configuration Selection Process

Step 1	Identify key aircraft design subsystems to evaluate the optimal configuration.
Step 2	Choose relevant FoM for analysis.
Step 3	Rate each option on a scale of 1 to 5 based on its strengths and weaknesses.
Step 4	Calculate total score for each option using L^2 norm and select the highest-scoring option.

Prototype construction informed the weighting of the scores, enabling the team to identify the factors with the most significant impact on aircraft performance and maintainability. A series of decision matrices was created to compare the various design options. These aspects included propulsion, landing gear configuration, empennage design, wing configuration and placement, wing planform, and XTV release mechanism. These analyses led the team to decide on a competition aircraft with a single-engine tractor configuration, tail-dragger landing gear, shoulder-mounted constant-chord wings, and a Hall effect release trigger.

3.4.1. Wing Type

Four wing structures were considered for the aircraft: monoplane, biplane, flying wing, and blended body. The key scoring criteria were aerodynamics, stability, drag, integrability, and manufacturability.

The most weighted FoM was the aircraft's aerodynamic characteristics to maximize flight efficiency for M2 and M3. In-flight stability was judged as coming secondary to ensuring the aerodynamics, as an aerodynamic aircraft necessarily implies some inherent degree of stability. The monoplane configuration was ultimately selected. Despite the biplane offering superior lift, it also introduces higher drag and more complex integration and manufacturing challenges. These drawbacks outweighed its aerodynamic benefits. In contrast, the monoplane provided a balanced solution with exceptional aerodynamics and easier manufacturability.

Table 5: Wing Type Decision Matrix

Wing Type		Monoplane	Biplane	Flying Wing	Blended Body
FoM	Weight	Score (1-5)	Score (1-5)	Score (1-5)	Score (1-5)
Aerodynamics	4	4	5	1	2
Stability	3	4	4	2	1
Drag	2	3	2	4	4
Integrability	3	5	3	2	3
Manufacturability	2	5	2	1	1
Final Score (L^2 norm)		15.97	13.82	7.87	8.94



3.4.2. Wing Location

Four different wing locations were considered: the standard high, shoulder, middle, and low wing positions. The FoM criteria were stability in flight, the integrability of the wing location into the design, and in-flight maneuverability. Stability was weighted the highest of these criteria, as an aircraft that consistently engages in stable flight is much more likely to successfully land, drastically improving scoring results. Second was integrability, as a straightforward wing attachment simplifies manufacturing and assembly, reducing complexity and potential points of failure. A high wing position was selected because it positions the center of gravity (CG) below the wing, improving roll stability.

Table 6: Wing Location Decision Matrix

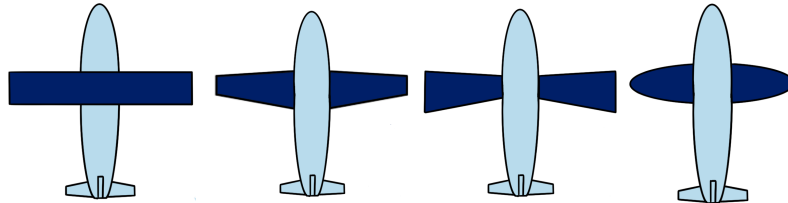
Wing Location		Shoulder Wing	High Wing	Middle Wing	Low Wing
FoM	Weight	Score (1-5)	Score (1-5)	Score (1-5)	Score (1-5)
Stability	5	4	3	3	2
Integrability	4	3	5	3	3
Maneuverability	2	2	3	4	5
Final Score (L^2 norm)		11.14	12.77	10.63	10.30

3.4.3. Wing Planform

Four different wing planforms were taken into consideration: constant chord, trapezoidal taper, reverse taper, and elliptical. The FoM that was assigned the most weight was manufacturability, as creating the wing is the most intensive manufacturing process on the aircraft. This year's design maximized the wingspan available within the competition requirements, to ensure maximum lift production. The simplest shape was chosen to ensure the repeatability and achievability of design of the manufactured parts. Although the flight characteristics of a constant chord wing may be inferior, all the ribs are identical and the spars have a constant height, improving their manufacturability compared to more complex planform shapes.



Table 7: Wing Planform Decision Matrix

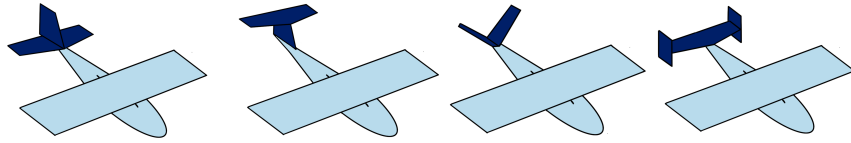


Wing Planform		Constant Chord	Trapezoidal Taper	Reverse Taper	Elliptical
FoM	Weight	Score (1-5)	Score (1-5)	Score (1-5)	Score (1-5)
Lift Efficiency	3	3	3	3	5
Induced Drag	2	3	4	4	5
Roll Moment	2	3	3	2	4
Manufacturability	4	5	2	2	1
Final Score (L^2 norm)		12.77	9.64	9.11	12.69

3.4.4. Empennage

The shape of the tail and structure of the empennage were chosen considering mission-specific factors. The configurations under consideration were conventional tail, T-tail, V-tail, and H-tail. The FoM include stability, maneuverability, drag, wake interference, and manufacturability. Stability was the most heavily weighted FoM because the empennage plays a critical role in maintaining straight and level flight, which is essential for controlled aircraft behavior. Enhanced stability reduces pilot workload and minimizes the risk of stalling or spinning, allowing for more precise control and efficient energy use. After thorough evaluation, a conventional tail configuration was chosen for this year's competition due to its ease of manufacturability, improved drag characteristics, and superior stability.

Table 8: Empennage Decision Matrix



Tail Configuration		Conventional Tail	T-Tail	V-Tail	H-tail
FoM	Weight	Score (1-5)	Score (1-5)	Score (1-5)	Score (1-5)
Stability	5	5	4	2	3
Maneuverability	4	4	4	3	4
Drag	4	5	4	3	3
Wake Interference	2	3	5	4	4
Manufacturability	3	5	4	2	1
Final Score (L^2 norm)		19.54	17.49	11.66	13.42



3.4.5. Propulsion

The propulsion configurations evaluated were twin tractor, single tractor, pusher, and ducted fan. Key FoM included weight, velocity, efficiency, and cost. Velocity was the top priority due to its critical role in maximizing performance in M2 and M3. Although efficiency and weight were also highly influential, they were secondary to velocity, as a heavy or inefficient aircraft that still achieves high speed meets the performance goals. Ultimately, the single tractor configuration was selected as the optimal choice.

Table 9: Propulsion Decision Matrix

Propulsion Configuration		Twin Tractor	Single Tractor	Pusher	Ducted Fan
FoM	Weight	Score (1-5)	Score (1-5)	Score (1-5)	Score (1-5)
Weight	3	3	5	5	2
Velocity	4	5	4	2	5
Efficiency	3	5	5	3	3
Cost	1	4	5	4	2
Final Score (L^2 norm)	14.76	15.46	11.58	11.96	

3.4.6. Landing Gear

Four landing gear configurations were evaluated: tricycle, quadricycle, tail-dragger, and wing-mounted. The selection process considered weight, manufacturability, induced drag, ground maneuverability, and pitch angle. Choosing the right landing gear is crucial, as it endures the highest stress during the most critical phases of flight—takeoff and landing. The tail-dragger configuration was the top choice due to its superior pitch angle on the ground, enabling shorter takeoffs.

Table 10: Landing Gear Decision Matrix

Landing Gear Configuration		Tricycle	Quadricycle	Tail-Draagger	Wing Mounted Landing Gear
FoM	Weight	Score (1-5)	Score (1-5)	Score (1-5)	Score (1-5)
Weight	4	4	3	5	3
Manufacturability	3	4	2	5	3
Drag	2	3	2	5	2
Stability	1	4	5	3	4
Takeoff pitch	5	2	3	5	3
Final Score (L^2 norm)	12.88	11.22	18.95	11.49	



3.4.7. XTV Release Detection Mechanism

The team considered several methods of detecting the release of the XTV. The methods considered include limit switches, wires that disconnect from another wire within the aircraft, an ultrasonic sensor, and a Hall Effect sensor. FoMs considered included the weight, manufacturability, reliability, and complexity of each mechanism. The Hall Effect Sensor proved to be the best balance between reliability and weight.

Table 11: XTV Release Decision Matrix

Payload Electronics Configuration		Wire Disconnect	Ultrasonic Sensor	Hall Effect Sensor	Limit Switch
FoM	Weight	Score (1-5)	Score (1-5)	Score (1-5)	Score (1-5)
Weight	4	4	2	5	3
Manufacturability	2	4	2	5	3
Reliability	3	1	2	5	2
Complexity	1	4	5	3	4
Final Score (L^2 norm)		10.72	7.81	15.30	9.06

3.5. Final Conceptual Design Configuration

Based on rankings conducted in the decision matrices, the final configuration was selected. Single monoplane wings were determined to be the easiest to implement and manufacture while offering a great deal of stability. High wings were chosen since the high placement in relation to the wing mount creates roll stability and allows for easier access to the electrical components. Constant chord wings were chosen in light of manufacturability. A conventional tail empennage was selected due to its high stability. A single tractor propulsion layout was chosen for its compliance with the modular design. The tail dragger landing gear was picked due to its takeoff performance. Lastly, a Hall effect sensor release detection mechanism was chosen for its good balance of desirable qualities.

A final conceptual sketch was created in preparation for preliminary design work, as shown in Fig. 8.



Figure 8: Final Conceptual Sketch



4. Preliminary Design

In the preliminary design phase, the CU AIAA team determined the initial aircraft configurations and overall sizing to satisfy mission requirements. The configuration of the wing geometry, landing gear, empennage, propulsion system, etc., was chosen during this stage of the design process. Subsequent design changes were performed upon further analysis and physical test results.

4.1. Design and Analysis Methodology

The CU AIAA design methodology is an iterative process based on the team's previous experience and other established methodologies. The team started the aircraft design process by deriving design requirements from the given mission requirements and conducting scoring analysis, as shown in Section 3.2 and Section 3.3 respectively. A preliminary weight estimation was conducted to determine the design space. Various trade studies were conducted to select the optimal aircraft configuration. An iterative approach was adopted to implement further design modifications based on simulation results from software including SOLIDWORKS, XFLR5, and AVL. The propulsion system was selected based on sensitivity analysis results to provide sufficient thrust for takeoff and efficient cruise. After completing detailed design, the team started manufacturing the aircraft. This involved 3D printing subcomponents and laser cutting wooden components. Wind tunnel testing was performed to assess airfoil and fuel tank bottle selection. After final assembly, static thrust, flight and ground tests were conducted, and the obtained results were compared with the initial design requirements. This process is shown in Fig. 9.

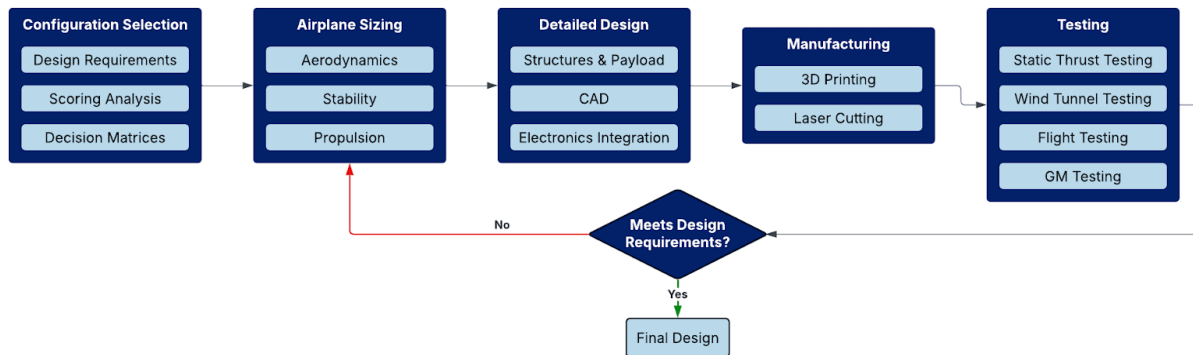


Figure 9: CU AIAA Design Methodology

4.2. Design and Sizing Trade Studies

Early in the CU AIAA design methodology, design and sizing studies were performed to find the optimal configuration such that the aircraft's overall performance will excel given competition rules and constraints. These studies provided the initial baseline on which further designing and prototyping was based.

4.2.1. Airfoil Studies

The first step of the design trade study process was airfoil selection. Proper airfoil selection is critical to the optimal performance of the aircraft due to the speed and payload incentives, as well as the restrictions on wingspan. With these considerations in mind and given the results of the sensitivity analysis, the choice was made to optimize for a high coefficient of lift (C_L) at low (~500,000) Reynolds number (Re)



flow and for a large range of angles of attack (AoAs) where the coefficient of lift to coefficient of drag ratio (C_L/C_d) is greater than 80. The first of these criteria prioritizes lift in the flow regimes the aircraft is expected to encounter, while the second criteria is aimed at maximizing stability in flight.

A search through the literature on low Re airfoils and the *Airfoil Tools* database gave two main candidates: the S1223 and the S7055 [2]. The S1223 is a well-known airfoil optimized for low Re flight, with superior lift and drag characteristics due to a cambered airfoil design. The S7055 is derived from the same family of airfoils and maintains some of the same stability and high lift in the low and extremely low Re regimes, but has a convex design which greatly simplifies manufacturing. When making the final determination, this convex shape was a large positive for the S7055, as it would allow for the use of MonoKote.

Though the S1223 airfoil has a significantly greater lift coefficient than the S7055, it carries several key downsides, the greatest being the infeasibility of manufacturing due to its very large camber. Beyond this, the S1223 also poses significant risks of stall at the large AoAs necessary in the takeoff and climb phase of flight. The S7055 airfoil, in contrast, has a far more stable decline in the C_L at higher AoAs while maintaining a similar, if slightly lesser, maximum C_L . The choice of the S7055 thereby maximizes both stability, while maintaining the capability to generate sufficient lift for a heavy payload.

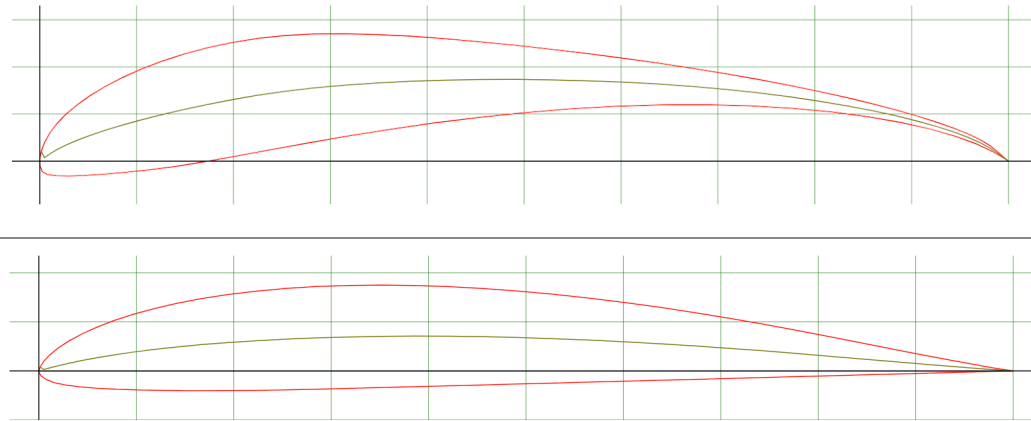


Figure 10: Candidate airfoil geometries. Top: S1223 airfoil—the high camber produces superior lift characteristics at moderate Re flow, but is impractical to manufacture. Bottom: S7055 airfoil—this airfoil maintains much of the lift profile while requiring minimal camber.

4.2.2. Wing Sizing Studies

The primary considerations when making decisions on wing sizing was the stability of the craft and total lift capacity in accordance with the sensitivity study. Beyond maximizing the wingspan within the competition guidelines of 6 feet, thereby maximizing lift and roll stability, the primary factor in determining the wing sizing was the aspect ratio (AR) of the wing, which would ideally be kept between 5 and 7 to reduce induced drag and increase roll control. Within this range, a lower aspect ratio was preferred to maximize area—and therefore lift—while also deferring stall until a greater AoA. Ultimately, an AR of 5 was chosen for the wing based on an analysis of various ARs presented in *Aircraft Design: A Conceptual Approach* [4], which demonstrates that an AR of 5 results in a high C_L as a function of AoA, while still remaining relatively consistent as lift peaks. Based on this AR, the chord length was chosen to be 14 in.



4.2.3. Control Surface Sizing Studies

Given that the primary goals of control surface sizing are maneuverability and controllability, relatively large control surfaces were chosen to provide the necessary roll and yaw control. This design choice was in part motivated by the lack of maneuverability observed in past CU AIAA aircrafts. To simplify manufacturing and minimize disruption to the airflow, flaperons are used. The flaperons each span approximately 45% of the single-wing wingspan to maximize control [4]. As such, the length of the flaperons is 16 in and the chord length is 2.25 in.

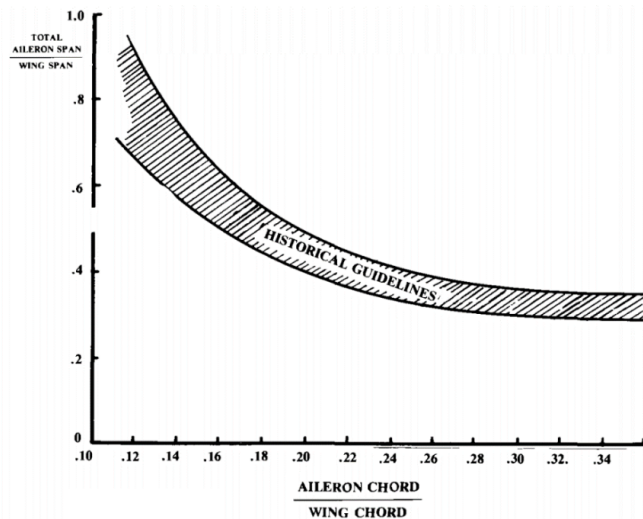


Figure 11: Aileron Size Graph

4.2.4. Tail Sizing Studies

Sizing of the tail was also based on good practices from [4]. The sizing of the tail is based primarily on the AR and tail moment arm. Specifically, guided by [4], the team decided to make the elevator chord 36% of the horizontal stabilizer chord, and the rudder chord 46% of the vertical stabilizer chord. The AR of the horizontal stabilizer was made to be less than that of the wings to delay the onset of stalling at high AoA; the stabilizer surface area is tied both to this AR and to the tail moment arm. The tail moment arm is defined as the distance from the quarter of the tail chord (of the mean chord, as measured from its leading edge) to the wing quarter chord. It is recommended that the tail moment arm of both the horizontal and vertical stabilizers be around 50-55% of the total airframe length.

4.2.5. Propulsion Studies

The selection of the propulsion system was focused on maximizing thrust while maintaining adequate power supply for each mission. Experience from last year's competition informed this decision due to the system being underpowered, resulting in poor flight performance.

A major constraint for propulsion design was the compliance of the battery with Federal Aviation Administration (FAA) regulations regarding the transportation of LiPo batteries on commercial flights. A 4500 mAh, 22.2 V (6S) LiPo battery would provide the power and capacity needed while still adhering to competition requirements of capacity less than 100 Wh.



The team researched several lower Kv rated motors relative to previous motors since lower Kv motors provide a higher torque, allowing for a larger propeller which would better provide the thrust needed to propel the aircraft. A range of motors from 450 Kv to 160 Kv was considered.

Tests with several different diameters and pitches of propellers were conducted to maximize the thrust provided by the motor. A range of propellers from 16x6E to 17x8E were tested. Based on these test results, a propeller of 16x6E was chosen, with the propeller producing 13 lbf of thrust.

4.2.6. Payload Studies

The aircraft's fuel tanks for M2 and M3 are required to be off-the-shelf beverage bottles. Initially, a square-shaped Pure Leaf Tea™ bottle was considered for its large flat sections, but it proved difficult to stop the adapter from sliding off the end of the bottle. Second, a Snapple™ bottle was considered for its deep ridges that would allow for the use of zip ties to secure the bottle adapter. After testing, the team decided against this design as it was difficult to stop the bottle from rotating and the zip-ties would snap under high loads. After reading *Design, Build, Fly Question and Answer Number 4*, Question 3 the team strived to find a bottle that has a small uniform cross section—while having the minimum required volume of 16 fl oz—in order to fully enclose the perimeter of the bottle and secure the adapter with cyanoacrylate. [6]. Several bottles, such as Sparkling ICE™, Essentia®, and Hal's New York™, met these requirements, but Sparkling ICE™ had the smallest cross section, meaning it would likely generate the least drag. Wind tunnel testing was conducted and confirmed this assumption to be correct.

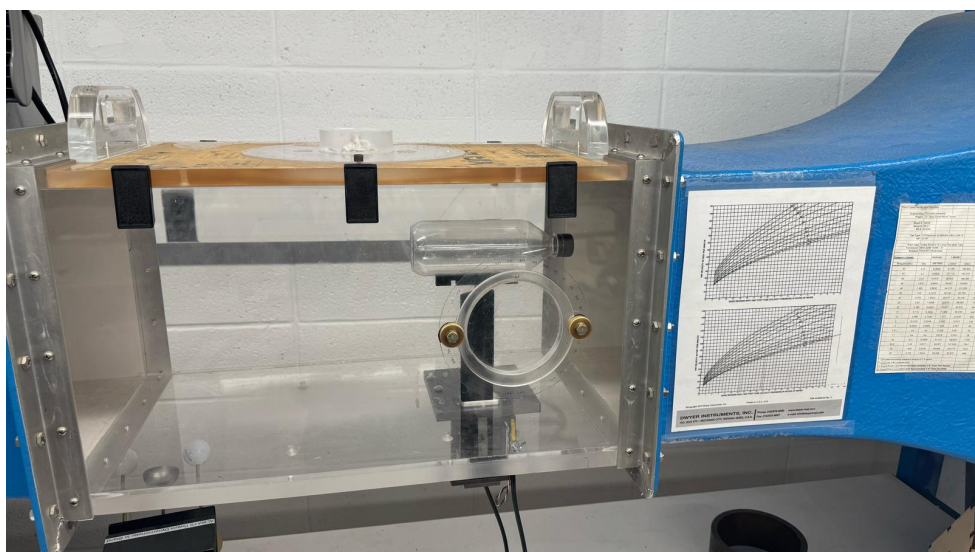


Figure 12: Wind tunnel testing was performed on potential bottles.

A spring-loaded quick-connect system, inspired by the Picatinny rails on firearms, was used to attach the fuel tanks. This system benefits from rapid connection and security due to its high strength springs. This system was compared with hardware-based alternatives that would have included M3x0.5 fasteners that would have been tightened during the attachment phase of the GM. A hardware-based system might be marginally more secure, however would be much slower to install. Considering the time requirements of the GM and the sensitivity study, this option was not chosen.



The fuel tank media considered included sand, water, rice, and metal scraps. Sand efficiently fills the space within the fuel tank and is dense enough to meet the desired weight. Its biggest drawback is that the electronics may be damaged if the bottle lid is not properly secured. Water has similar properties to sand but poses similar risks, and is also less dense. Rice poses no threat to the electronics, which is a considerable benefit over the other media, and has an overall density not far behind water. Metal scraps have the greatest mass but are inefficient in their packing density. Metal also risks shifting around when isolated in the bottle. This evaluation led to the choice to combine rice and metal. Inserting a rod of steel into the bottle before filling the rest with rice creates a fuel tank with the ideal mass, without any worry of the mass shifting around or damaging electronics.

A potential design for the XTV was building one based on the Flite Test “Sparrow” model, but considering the incentive to make the XTV as light as possible the team decided to pursue a pre-made expanded polyolefin (EPO) foam glider with the motor and receiver removed. This would enable the use of small 2 gram servos that would otherwise be very challenging to implement. The XTV is further modified with sections removed to allow for the Global Positioning System (GPS) electronics and the strobe lights.

4.3. Performance Prediction Methodology

A variety of factors went into predicting the performance and overall score of *Carrier Pigeon*. It was vital to ensure that every step of the flight was fully understood to confirm that all simulations, analyses, and tests were relevant to the prediction data required.

4.3.1. Description and Capabilities

For M1, M2, and M3, the aircraft follows the same flight path. The flight path can be divided into several parts, each with its own unique flight characteristics:

- Takeoff
 - Takeoff is performed near maximum throttle, with control surfaces in a high lift configuration. The motor remains near maximum thrust while the aircraft climbs to its cruising altitude.
- Level Cruise
 - This is a straight and level flight. Motor speed is configured to maintain speed at the AoA necessary for level flight. Flaperons are used in conjunction with the rudder to compensate for roll and yaw moments, respectively.
- Banked Cruise
 - Flight at this stage is still level. However, due to centripetal acceleration, the throttle is decreased to allow for tighter turns without exceeding the maximum safe acceleration. Flaperons are used to control banking.
- Approach and Landing
 - Altitude and speed are gradually bled off as the aircraft approaches the runway. To achieve this, the engines are run at lower power and eventually idled as the aircraft transitions into a flare near the runway threshold. A gentle landing is particularly important due to the extra weight of the payload in M2 and M3. The rudder and flaperons must be used to ensure a level landing.



4.3.2. Uncertainties

In the CFD characterization of the aerodynamic properties of the wing, several sources of uncertainty could have affected the accuracy of the results. These sources include the turbulence model used to represent the flow, the mesh type and resolution, and the boundary conditions specified to define the airflow around the wing. Additionally, imperfections in manufacturing introduce geometric uncertainties into airfoil surfaces, consequently introducing discrepancies between the CFD results and the true aerodynamic performance of the wing. Therefore, it is important to carefully evaluate and validate the CFD results against experimental data.

Many uncertainties may detrimentally affect actual airfoil performance. Crabbing from any crosswinds will increase flight time, as well as headwinds that decrease ground speed for a given airspeed. Estimates for the reference score of the top-performing team are also subject to significant change and uncertainty. Finally, environmental conditions in Tucson, such as barometric pressure and winds will likely vary significantly from those at CU AIAA's flight area in Teaneck, New Jersey; typical values taken from the National Weather Service are summarized below [3].

Table 12: Comparison of Weather Conditions

	Teanek, February (2025)	Tucson, April (2025)
Average Daily Temperature (Low/High)	34°F / 49°F	53°F / 83°F
Average Daily Precipitation	0.03 in (0.77 in total)	.01 in (0.24 in total)
Highest Daily Average Wind Speed	10.3 mph	8.7 mph
Average Cloud Cover	52%	22%
Average Barometric Pressure	30.07 inHg	30.02 inHg

Aside from varying meteorological conditions, pilot performance also introduces uncertainty in the ultimate performance of the aircraft.

4.4. Aerodynamics and Stability Prediction

The aerodynamics and stability of the aircraft were studied through a combination of first-principles calculations, aerodynamic simulations, and iterative design given test-flight feedback. In cruising conditions, the dynamic stability of the craft was viewed with higher standards. Predictions were calculated using a combination of methods, including first-principles calculations and simulations in both AVL and XFLR5. These three distinct methods were cross-referenced to ensure robust prediction of the aircraft's aerodynamic performance and characteristics.

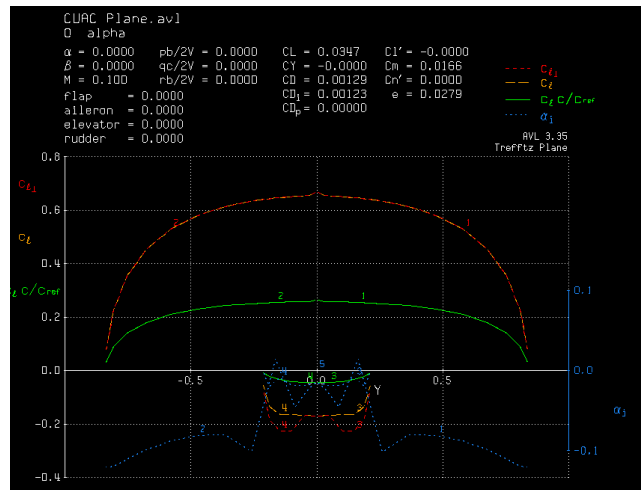


Figure 13: Trefftz Plot Produced Using AVL



Fig. 13 displays the coefficient of lift and the coefficient of drag as a function of wingspan, resolving the approximate amount of lift and drag induced at any specific distance in level flight. Downwash angles as a function of position along the wingspan are also shown. The even nature of all of the curves, with most of the lift produced near the center of the wing, predicts a high level of aerodynamic stability in yawing and rolling situations.

4.4.1. Static Stability

To ensure stable flight characteristics while cruising, the airframe was constructed to place the CG roughly below the aerodynamic center at 0.25 chord length, improving roll and pitch stability of the aircraft. Given the location and aerodynamic characteristics of the empennage, the neutral point can be calculated by setting the equation for pitching moment slope with respect to AoA.

$$C_{m\alpha} = C_{L\alpha}(\bar{X}_{cg} - \bar{X}_{acw}) + C_{mfa} - \eta_h \frac{S_h}{S_w} C_{Lha} \frac{\partial \alpha_h}{\partial \alpha} (\bar{X}_{ach} - \bar{X}_{cg}) + \frac{F_{pa}}{qS_w} \frac{\partial \alpha_p}{\partial \alpha} (\bar{X}_{cg} - \bar{X}_p)$$

from [4] equal to 0 using estimates and tabulated values from [2]. Note that in the above, all distances are with respect to chord length. Ultimately, a value of 0.45 is calculated for the neutral point. This gives a static margin of roughly 20%, which falls within the general practice range and indicates a sufficient stability against pitching in static flight conditions. One may also calculate the overall pitching moment derivative with respect to AoA, C_{Ma} , given that $\bar{X}_{cg} = \bar{X}_{acw}$, giving a value of -0.33, which is negative and further indicates stability to small deviations in the pitch.

Other static stability parameters for the coefficient of lift slope with respect to AoA ($C_{L\alpha}$), directional stability ($C_{n\beta}$) and lateral stability ($C_{l\beta}$), were calculated similarly, and are summarized in Table 13 below.

Table 13: Static Stability Summary (Angular Measure in Degrees)

Quantity	Static Moment	C_{Ma}	$C_{L\alpha}$	$C_{n\beta}$	$C_{l\beta}$
Value	20%	-0.33	0.1	0.002	0.0004

Further analysis of the stability of the airfoil's drag and lift characteristics was performed, with particular emphasis on both the takeoff and cruising regimes, corresponding to 50,000 and 200,000 Re flows, respectively. Given a takeoff AoA of around 11° and a cruising AoA of 6°, the following stability characteristics, particular to the wing, were calculated.

Table 14: Static Stability Summary of Airfoil

Category	Takeoff	Cruising
Lift Coefficient (C_L)	1.25	1.0
C_L Curve Slope [per %]	0	0.1
Lift-to-Drag ratio (C_L/C_D)	27	77
C_L/C_D Curve Slope [per °]	-5.0	0

In particular, the configuration takeoff corresponds to a maximum in the C_L curve, leading to more stable lift characteristics during takeoff. On the other hand, while cruising, the aircraft maximizes the lift to drag ratio, resulting in overall stable flight characteristics.



4.4.2. Dynamic Stability

The dynamic stability of the aircraft was analyzed using XFLR5 and comparing the results to military guidelines for piloted aircraft established in MIL-F-8785B. The guideline establishes different classes of aircraft, different flight phases, and acceptable value ranges for three levels of flight quality. *Carrier Pigeon* most closely matches Class I, defined as "Small, light airplanes." Additionally this analysis focuses on the main part of the flight, Category B, defined as "Those nonterminal Flight Phases that are normally accomplished using gradual maneuvers and without precision cracking, although accurate flight-path control may be required;" this includes climb, cruise and descent. The analysis considers five stability modes: two longitudinal modes (phugoid and short period) and three lateral modes (Dutch roll, roll, and spiral) (MIL-F-8785B: Flying Qualities of Piloted Aircraft, [5]).

Table 15: Dynamic Mode Level Classifications for Class I, Category B Flight

	Longitudinal Modes		Lateral Modes		
	Phugoid	Short Period	Dutch Roll	Roll	Spiral
Level 1	$\zeta > 0.04$	$0.3 < \zeta < 2$	$\zeta > 0.08$	$T < 1.4$	$t_2 > 20$
Level 2	$\zeta > 0$	$0.2 < \zeta < 2$	$\zeta > 0.02$	$T < 3$	$t_2 > 12$
Level 3	$t_2 > 55s$	$0.15 < \zeta$	$\zeta > 0.02$	$T < 10$	$t_2 > 4$

Table 16: Dynamic Stability of the Aircraft

Mode	Eigenvalue	Damping Ratio	Half Life (s)	T (s)	Level
Phugoid	$-0.0016 \pm i0.5430$	0.00297948	/	/	2
Short Period	$-9.2658 \pm i9.3438$	0.704135	/	/	1
Dutch Roll	$-1.5127 \pm i6.5978$	0.223477	/	/	1
Roll	-17.3806	/	0.0398806	0.0575355	1
Spiral	0.0473	/	-14.6475	/	2

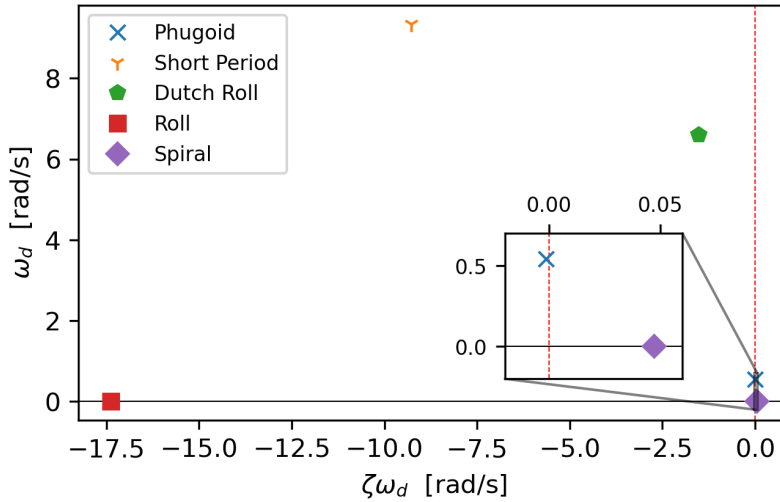


Figure 14: Mode root locus plot. An inset zoom of the spiral and phugoid modes is included.

The results of the XFLR5 stability analysis, shown in Table 16 and Fig. 14, indicate that the real parts of all eigenvalues are negative, except for the spiral mode which has a small real part i.e. all modes are damped except the spiral mode which is slightly divergent. However, the magnitude of this anti-damping is extremely small, implying that it may easily be corrected with active pilot input. This is consistent with the MIL-F-8785B flight quality level 2 standard—which indicates “flying qualities adequate to accomplish the mission, but some increase in pilot workload”—and is thus acceptable for the mission being flown [5].

4.4.3. Flight Predictions

Using the definitions of the aerodynamic coefficients,

$$C_L = \frac{L}{q_\infty c} \quad C_D = \frac{D}{q_\infty c}$$

first-principles total lift and drag forces may be computed from the tabulated values of C_L and C_D —shown in Fig. 15—at the expected cruising AoA of 6° . To confirm the first-principles calculations of lift and drag the team ran a CFD simulation using XFLR5. The drag, lift, airflow, and pressure across the airfoil (see Fig. 16 below) were analyzed, modeling the externals of the wings including the flaperons in multiple positions. The simulation results showed close agreement within 10% of first principles calculations. The predicted performance is given in Table 17.

Table 17: Predicted Aerodynamic Performance

	F_{Lift} [lbf]	F_{Drag} [lbf]
First Principles	26.4	1.0
Simulated	26.0	1.1

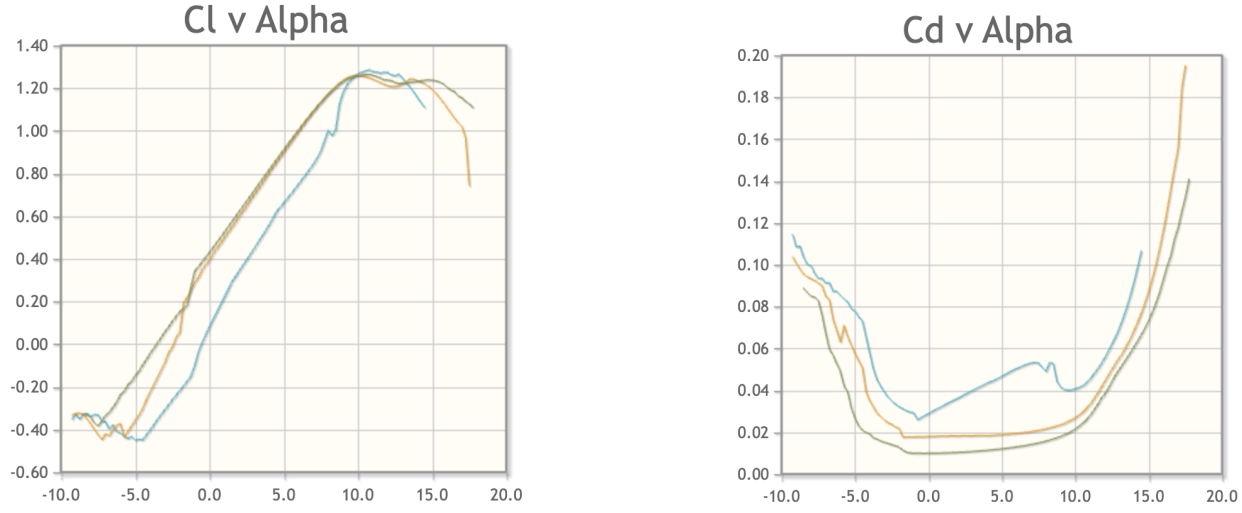


Figure 15: Lift/drag coefficients; different lines show Re ranging from 10,000–500,000.

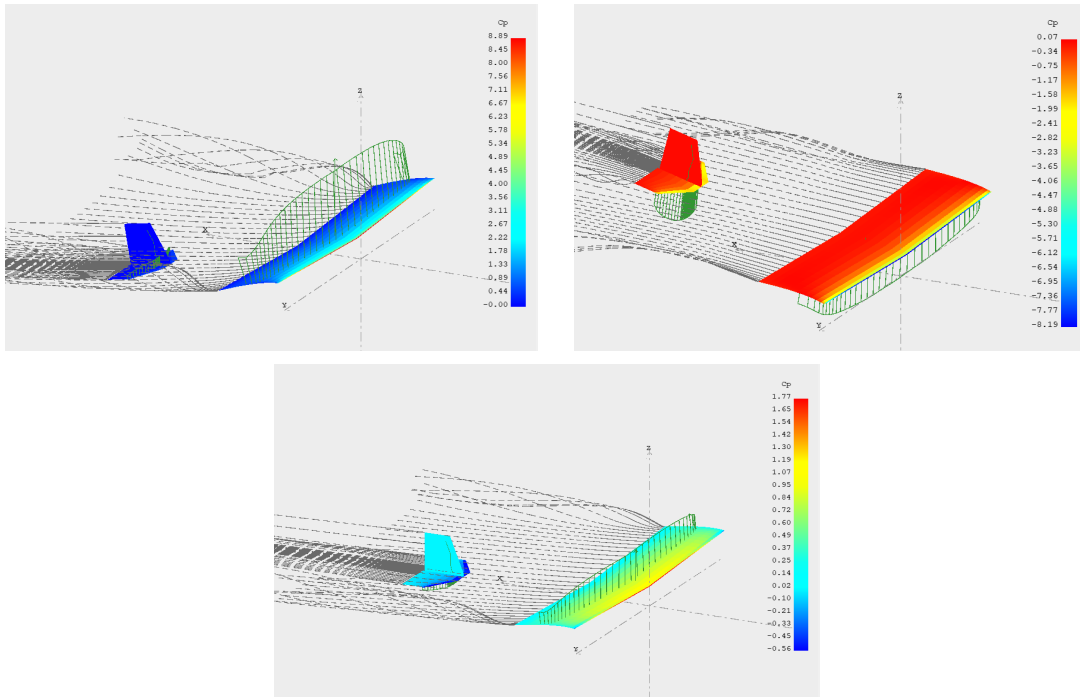


Figure 16: Wing aerodynamic flow simulation. From left to right $+10^\circ$, 0° , and -15° inclined flight is shown

4.5. Mission Performance Estimation

Using the simplified mission model programmed in Python, updated with the aerodynamic qualities predicted by the aerodynamic analysis, estimated mission performances were calculated. These estimated performances are given in Table 18 below. Note that the M3 raw mission score includes the assumption of a successful XTV drop scoring the 2.5 possible bonus points. The mission scores are reported as a raw additional score, i.e. the non-constant part of the score pre-normalization.



Table 18: Predicted Mission Performance

Quantity	M1	M2	M3
Payload Mass (Fuel/XTV) [lb]	0	4	3
TOW [lb]	6	11	9
Cruise Throttle	70%	95%	95%
Cruise Speed [ft/s]	56	63	66
Battery Usage	34%	40%	92%
Lap Number	3	3	8
Mission Time [s]	150	121	289
Completion Score	1	1	2
Additional Raw Score	0	1.98	11.5

5. Detailed Design

Following the conceptual and preliminary design phases, the detailed design was performed. This involved extensive analysis and testing of specific component selections and configurations, both on the ground and in flight, to ensure the aircraft's readiness for competition. A particular focus was placed on weight reduction, with careful consideration given to the potential impacts on aircraft performance and structural integrity.

5.1. Dimensional Parameters of the Final Design

Table 19: Final Dimensional Parameters

General Parameters								
Total Length	71.0 in	Total Wingspan		70.0 in	Empty Weight		5.64 lb	
Aerodynamic Surfaces				Control Surfaces				
	Wing	Horizontal Stabilizer	Vertical Stabilizer		Flaperon	Elevator	Rudder	
Airfoil	S7055	Flat Plate	Flat Plate	Chord [in]	2.25	2.52	2.75	
Span [in]	70.0	20.0	9.19	Span [in]	16.0	20.0	8.50	
Chord [in]	14.0	7.50	7.50	Area [in ²]	36.0	50.4	22.3	
Area [in ²]	980	162	69.7					
AR	5.00	2.46	1.03	Moment Arm [in]	27.0	24.4	24.3	
Incidence Angle [°]	5.00	0.00	0.00					
Propulsion								
Battery	Motor		ESC		Propellers	Receiver	Transmitter	
HRB Power 4500mAh 6S 22.2 V 100C LiPo Battery	Spektrum Avian 5065-450Kv Outrunner Brushless Motor		E-flite 100-Amp Brushless ESC, 2-6S		16X6E	FrSky X8R	FrSky QX7 Taranis	



Figure 17: Final Design of *Carrier Pigeon*

5.2. Structural Characteristics and Capabilities

The aircraft structure was designed to balance strength, weight, and aerodynamic performance. The primary load-bearing components, the wing, motor mount, and empennage, were engineered to withstand the expected aerodynamic and inertial forces encountered during flight. The control surfaces are integrated with reinforced hinging to ensure smooth and reliable actuation. The central carbon fiber rod serves as the structural core, supporting the modular integration of aircraft electronics and payloads while distributing loads effectively across the airframe. Designed to handle high-g maneuvers and landing stresses, the structure ensures both durability and stability under operational conditions.

5.3. Subsystem Design

The subsystems were meticulously designed to meet the specific performance and structural requirements of this year's competition. FEAs were conducted on critical components to ensure they could withstand operational forces and maintain reliability throughout flight. Each system was optimized for efficiency, durability, and seamless integration within the overall airframe.

5.3.1. Wing Mount

The central design element of *Carrier Pigeon* is the 3D printed wing mount. This structure joins the two carbon fiber wing spars and locks them into place with cotter pins. The wing mount consists of a top section and bottom section, with a square cutout where the two meet that allows the mount to slide onto the aircraft's carbon fiber structural rod. The two sections clamp together using 8-32 nuts and bolts to prevent the wing mount from translating along the structural rod, while enabling adjustability.

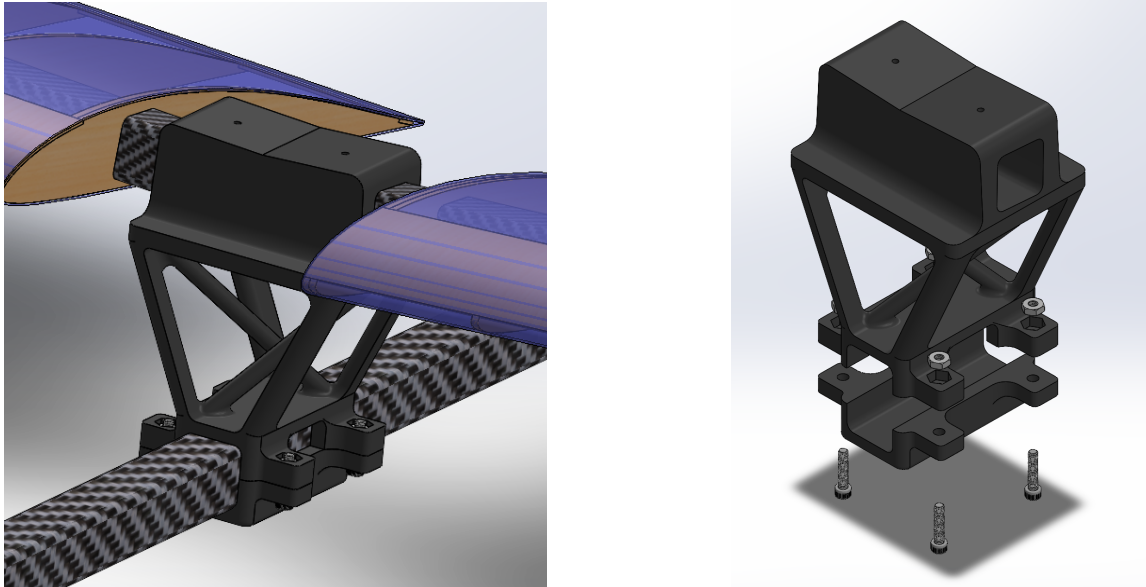


Figure 18: Wing Mount (Left: Assembled with Wings, Right: Exploded View with Hardware)

As this is the most critical structural piece of the aircraft, extensive FEA was performed. The estimated mass of the aircraft during M2 is approximately 10.7 lb. With that in mind, based on past results, the maximum estimated acceleration experienced by the aircraft is around 6 g. Therefore, the maximum force experienced by the aircraft can be estimated as 64.2 lbf. To simulate this load, it is assumed that the force acts uniaxially in the direction of gravity.

Given the anisotropic behavior of printed Polylactic Acid (PLA) and the general difficulty of conducting FEA on Fused Deposition Modeling (FDM) parts, simplified material properties for PLA were obtained based on the specific infill density, infill geometry, and print orientation (Mechanical Properties, [7]), as well as the datasheet for Bambu Lab PLA Filament [8].

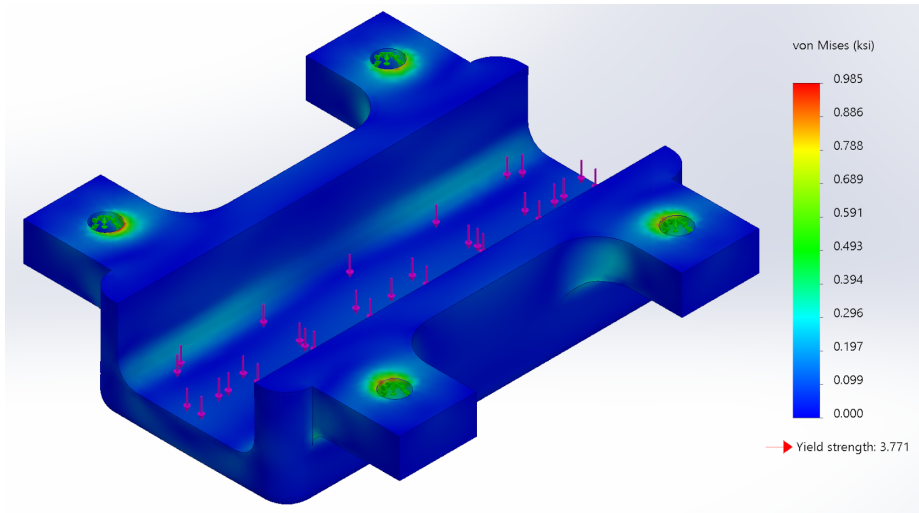


Figure 19: Wing Mount Bottom Section FEA



Fig. 19 shows that the maximum stress experienced by the wing mount bottom section, 0.985 ksi, is well below the yield strength of 3.771 ksi. According to the von Mises stress criterion, this design has a minimum Factor of Safety (FOS) of over 3. This FOS is necessary given the large uncertainties of FEA on FDM parts.

A similar analysis was performed for the top section of the wing mount. The bottom of the piece was fixed while the loading was applied upward to simulate the lift from the wings. A load of 66 lbf was assumed at the top inner face of the square wing spar cutout to account for the moment produced by lift on the wings.

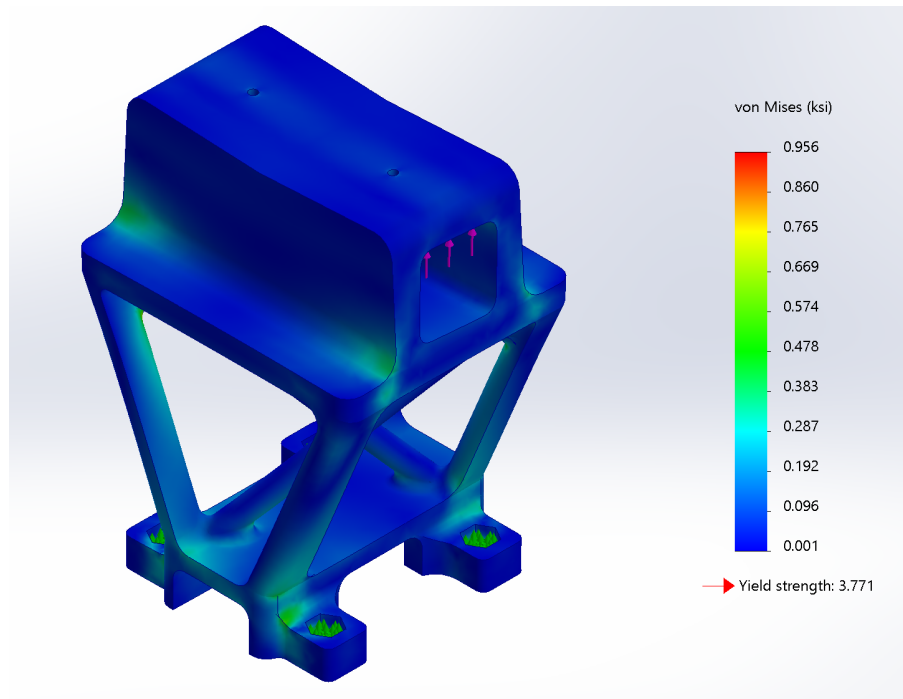


Figure 20: Wing Mount Top Section FEA

From Fig. 20, it can be seen that the top section of the wing mount has a minimum FOS of around 4 according to the von Mises criterion. These results give confidence that the piece can withstand the expected loads while accounting for uncertainties in the analysis.

5.3.2. Carbon Fiber Rod

The 1.07 in wide carbon fiber rod running along the longitudinal length of the aircraft acts as the central structural feature connecting all the other components together. Attached to the rod are the three main components of the aircraft: the wings, the empennage, and the landing gear. Additionally, components such as the motor and battery are separately attached to the rod. The primary goal of the design was to maximize stability, minimize weight, and maintain structural integrity throughout flight, takeoff, and operations.

5.3.3. Wings

The wing skin was made from heat-shrunk sheets of MonoKote. Structural rigidity and dimensional stability are provided by a single 1 in square carbon fiber spar running through laser-cut 0.125 in thick



balsa ribs. Additional 0.0625 in balsa wood sheets were placed along the leading and trailing edges of the wing to provide structural integrity and to help maintain the airfoil profile. The wing mount was 3D printed out of PLA, with the carbon fiber spars press-fit and secured with cotter pins that go through them. Control surfaces were made from 0.125 in sheets of plywood.

A FEA was performed on the full wing assembly to verify the structural integrity of the materials chosen for the wing's internal design. With a force of 60 lbf, the wing experiences a maximum deformation below 0.1 in, with a FOS of 2.8.

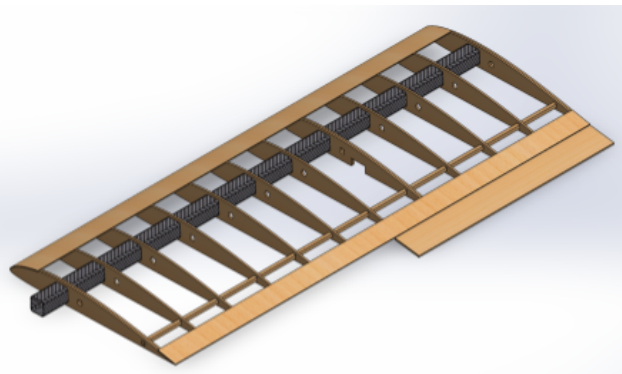


Figure 21: Wing Internal Design.

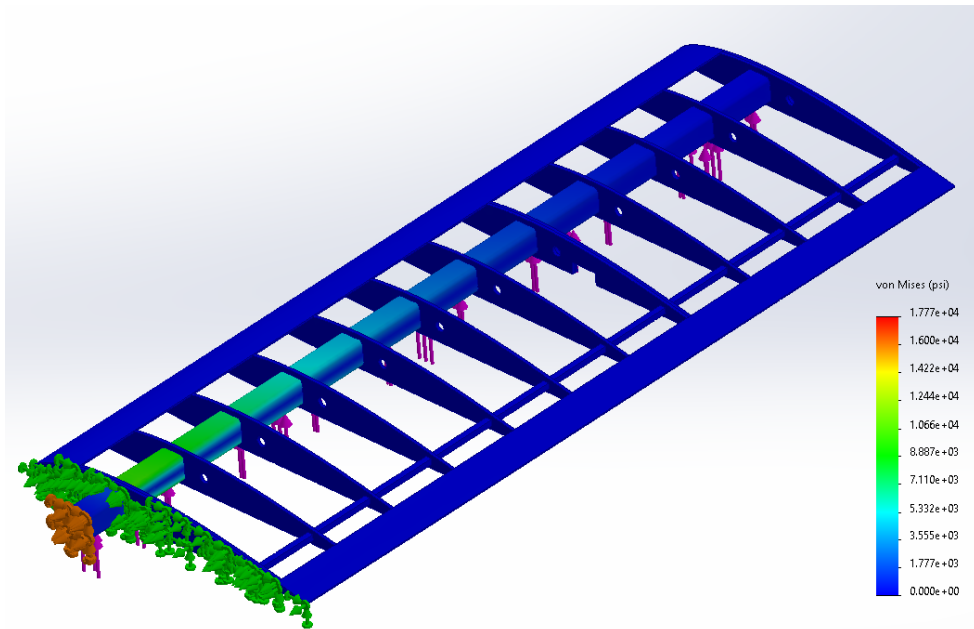


Figure 22: Wing FEA

5.3.4. Empennage

The empennage is composed of two laminated sheets of foam board for the horizontal stabilizer and the vertical stabilizer. The vertical stabilizer is connected to the horizontal stabilizer using epoxy and two thin carbon fiber rods. This system is extremely compact and easily slides onto the main structural rod, enabling rapid assembly.

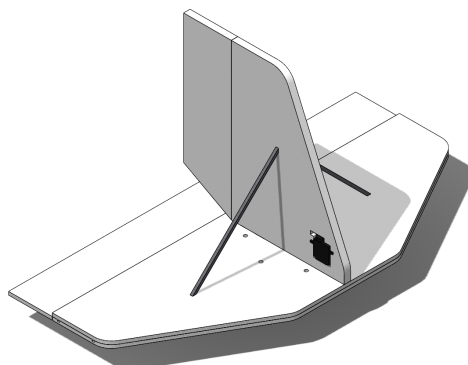


Figure 23: Empennage Design



5.3.5. Landing Gear

For the landing gear, a non-retractable taildragger configuration was chosen to minimize complexity. Given that the vibration and shock from takeoff/landing were not major concerns in this competition, a suspension system was omitted to save weight and avoid complexity. The front landing gear is an off-the-shelf part made of carbon fiber, mounted onto the structural rod by a PLA 3D print. The landing gear mount was designed with the intention of fastening the front landing gear, maintaining a lightweight build without sacrificing security. The landing gear is bolted onto the mount and modularly attached to the structural rod. The tail wheel is an off-the-shelf caster wheel also mounted onto the structural rod by a PLA 3D print. The landing gear together create a motor pitch angle of 9.48° on the ground.

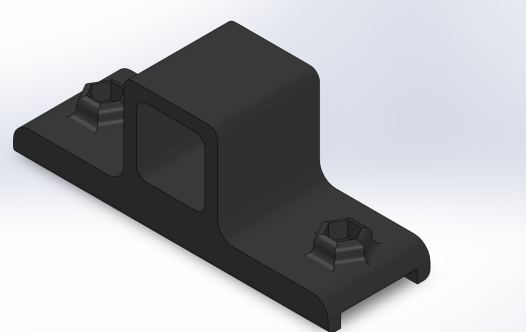


Figure 24: Landing Gear Mount Design

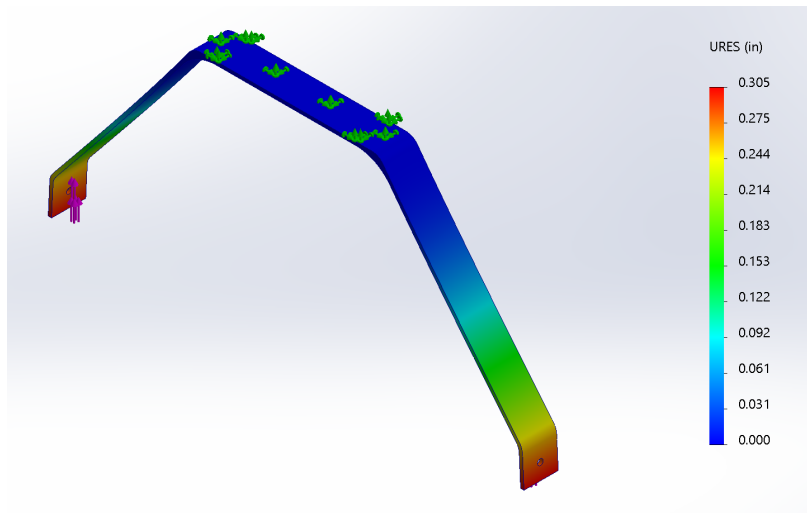


Figure 25: Landing Gear FEA

FEA was performed on the front landing gear to ensure that it can withstand the expected loads. To simulate these forces, the landing gear was modeled with a fixed region that attaches to the landing gear mount. 30.9 lbf loads were placed at the wheel axles, resulting in a maximum deflection of 0.305 in.

5.3.6. Electronics Compartment

The electronics compartment is located near the front of the aircraft and modularly attached to the top of the structural rod. This PLA 3D printed part contains the



Figure 26: Electronics Compartment Design



receiver and electronics battery, and externally holds the ESC. Since the aircraft does not have a central fuselage, it was essential to have a compartment to secure these parts. The electronics are accessible through a top hinge that is secured with adhesive nylon reinforced tape and velcro.

5.3.7. Motor Mount

The motor is mounted onto a PLA 3D printed component designed to fit securely onto the structural rod. One end of the mount slides onto the rod and is fastened with a screw that passes through pre-aligned holes on both the mount and the rod. The opposite end features a central hole for the motor shaft, along with 4 holes that align with the motor's backplate, allowing for secure attachment with screws. Hexagonal slots are integrated into the mount to hold nuts in place, preventing them from loosening during operation. The thrust test verified the structural integrity of the mount and confirmed that it can withstand the expected loads.

5.3.7. X-1 Test Vehicle

The XTV was built by modifying a Top Race Sky Eagle RC Plane. This was done by removing the front of the RC aircraft, exposing the internal components and removing the stock motor and battery. An Arduino Nano powered by a 9 V battery was used as the central interface for the guidance, flight control, and lighting systems. The guidance system consists of a GPS module and an Inertial Measurement Unit (IMU), and tracks the position of the XTV relative to a set of coordinates. With this information, the Arduino Nano then commands the aileron servo motor to guide the XTV towards the designated position. Additionally, a Hall Effect sensor detects when the XTV is released from the aircraft, triggering a blinking light mounted on the bottom of the XTV. Fig. 28 shows the schematic of the XTV's electrical system.

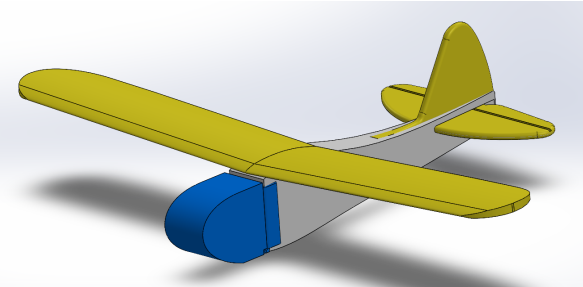


Figure 27: XTV Design

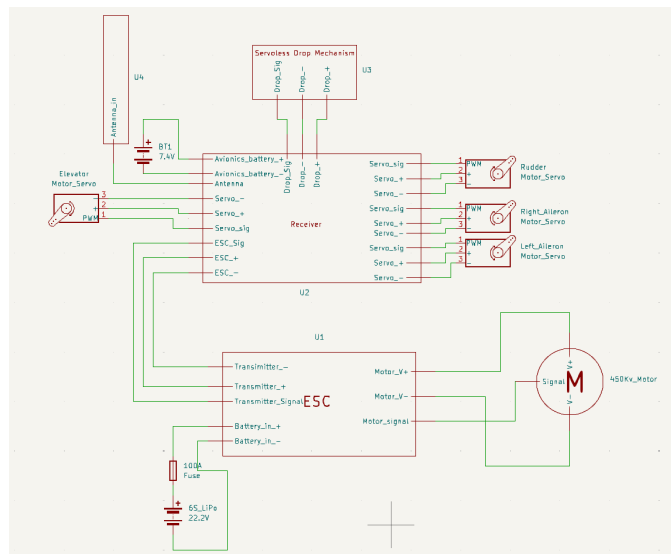


Figure 28: XTV Electronics Schematic



5.3.7. Fuel Tanks and Pylons

The pylon connects to both the aircraft and the bottle adapter with a spring-loaded rail mechanism. The system is based on a dovetail rail modeled after Picatinny rails used on firearms, as seen in Fig. 29. The female part of the mount has a spring that pushes a small section of the connecting piece out of place where there is a notch in the rail. That can be seen in Fig. 29 panels 2 and 3. This offset section slides into the notch and disrupts the linear movement of the assembly, as visible in the difference between panels 1 (unsecured) and 2 (secured) of Fig. 29. The displaced section must be manually squeezed to line up with the rest of the female assembly and allow for movement, as displayed in panel 4 of Fig. 29. This system is a positive locking mechanism as any compression of the springs makes them even harder to compress, ensuring security and safety when installing the fuel tanks. This design is intended to make installation as quick as possible and therefore a very strong spring was selected for the mechanism, requiring over 8 lbf to release, as removal is not a timed portion of the competition. The male part of the rails also features a hard stop that lines up with the female section being in the notch, which stops the sections from sliding too far into each other.

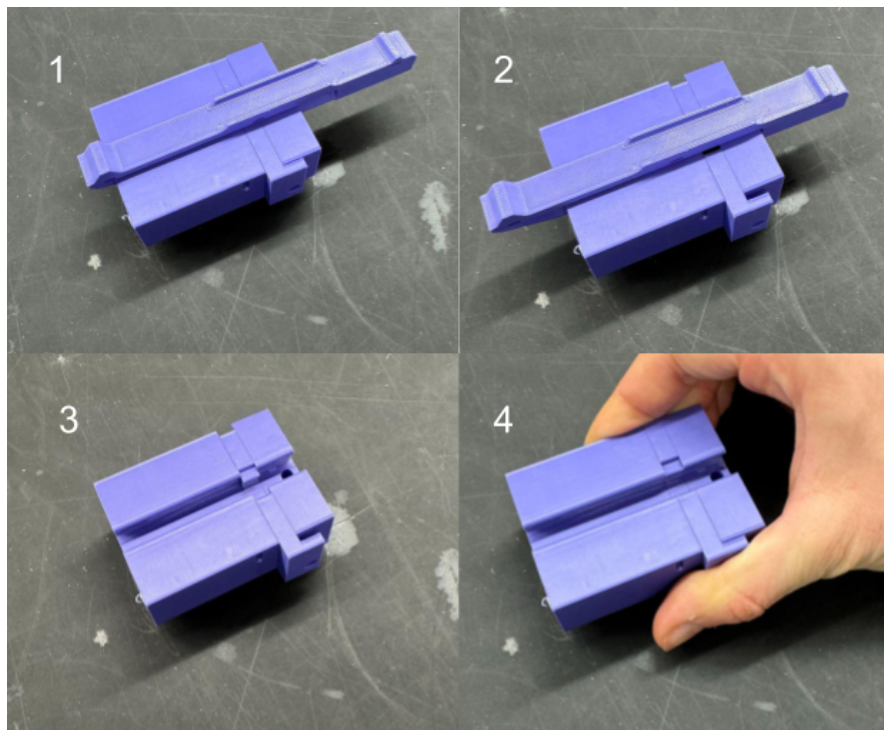


Figure 29: Pylon Mount States

5.4. Propulsion and Avionics Characteristics

One brushless direct current (DC) outrunner motor is installed along the centerline of the aircraft on the nose with an appropriately rated 100 A ESC inline with the structural rod of the aircraft. This motor provides approximately 13.01 lbf of thrust which gives a thrust-to-weight ratio of approximately 2 for the M1 configuration. The motor is powered by a single battery rated at 6S (22.2 V), as recommended by the manufacturer.

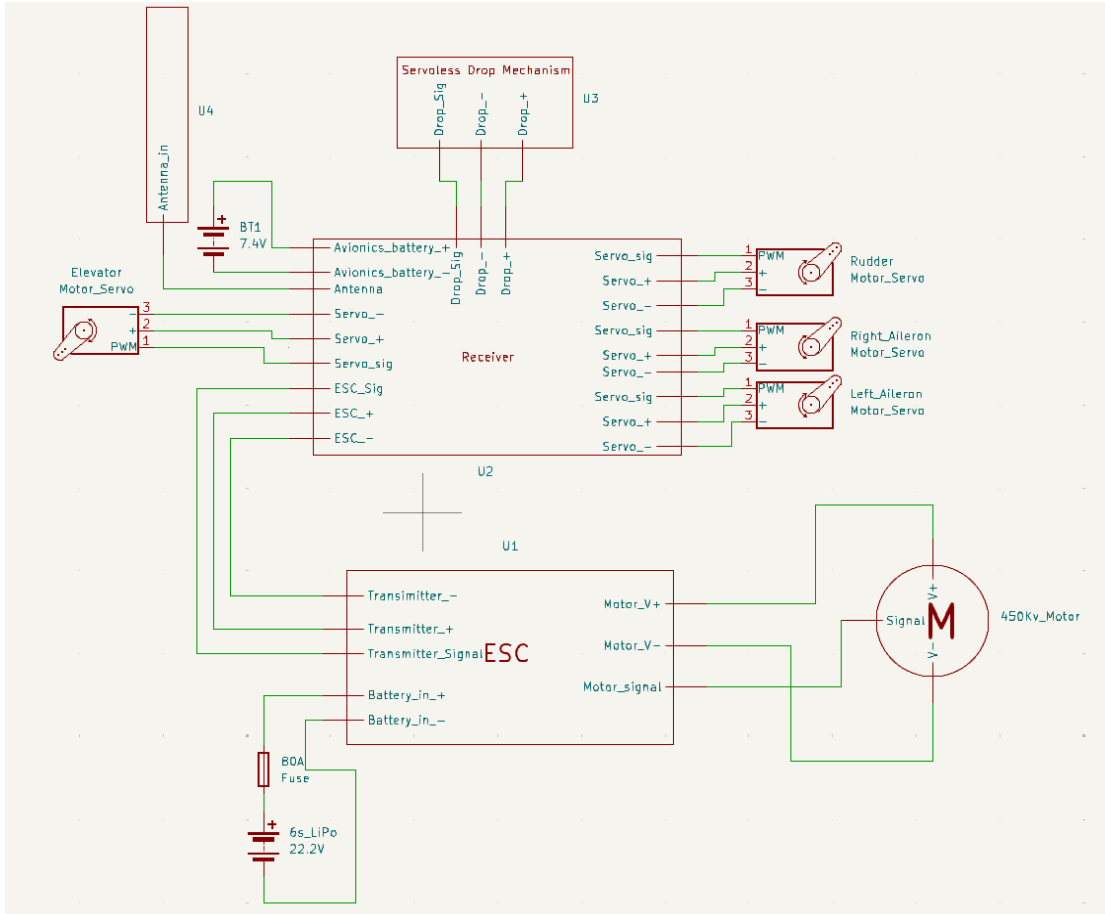


Figure 30: Propulsion and Avionics Schematic

The batteries were chosen based on expected duration, current draw, and flight time. The motor has a maximum current draw of 85 A, although the aircraft is expected to draw around 80 A in cruise. With a liberally estimated flight time of approximately 5 minutes (for the maximum component of aerial competition time), the necessary battery capacity was calculated to be within the durational limits:

$$\text{Battery Duration} = 99.9 \text{Wh}/1200 \text{W} \times 60 \text{ min/hr} = 4.995 \text{ min}$$

A rough estimation of motor performance is calculated below with a range of the motor's nominal Kv values and the battery's voltage rating which yields the motor's expected revolutions per minute (RPM).

$$\text{RPM} = 22.2 \text{V} \times \{450 \text{ Kv}\} = \{9,990\} \text{ RPM}$$



5.5. Weight and Balance

Theoretical weight and balance analyses were performed using SOLIDWORKS. The full assembly model of the airframe was assembled with relevant materials (and their densities). The following table presents the full results of the analyses, splitting the aircraft into relevant mission configurations. The origin of the weight and balance is at the front of the motor mount in the x- and z-directions, as shown in Fig. 31.

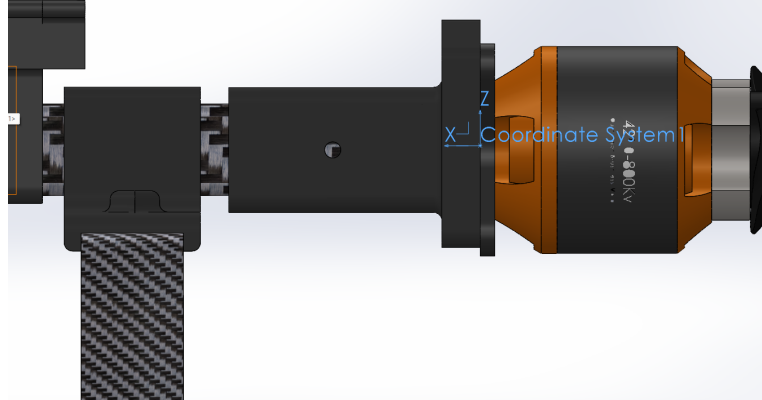


Figure 31: Full aircraft assembly CAD origin. +x points towards empennage; +z points away from landing gear.

Table 20: Weight and Balance Table

Mission	Component	Weight (lb)	x-displacement (in)	z-displacement (in)
General	Main Rod	0.55	30.40	0.00
	Motor + Propeller	1.32	-1.50	0.00
	Landing Gear	0.48	4.28	-7.48
	Electronics Compartment	0.27	7.35	1.27
	Wing Mount	0.33	17.25	4.07
	Wing	0.68	20.92	4.53
	Tail Wheel	0.08	51.59	-2.13
	Empennage	0.41	59.53	5.10
M1	Battery + Mount	1.52	11.63	-2.52
	Total Plane	5.64	16.87	0.62
M2	Battery + Mount	1.52	11.63	-5.49
	XTV Release	0.21	25.12	-2.10
	XTV	0.49	25.32	-5.38
	Pylon Assembly	0.36	16.28	0.20
	Fuel Tank x2 (Full)	4	21.35	-0.30
	Total Plane	10.7	19.87	-0.37
M3	Battery + Mount	1.52	11.63	-2.52
	XTV Release	0.21	25.12	-2.10
	XTV	0.49	25.32	-5.38
	Pylon Assembly	0.36	16.28	0.20
	Fuel Tank x2 (Empty)	1.26	12.43	0.13
	Total Plane	7.96	19.87	1.53



5.6. Predicted Flight and Mission Performance

Using the aforementioned aerodynamic properties, aircraft cruise speeds required to sustain a lift-to-weight ratio of 1 were calculated. These values were then used to estimate course completion time, which could in turn be used to predict mission performance. Ground mission performance was tested experimentally in-house. Extrapolating from mission high scores from previous years, projections for mission performance maxima were estimated. The final, normalized score shown in Table 21 was estimated to be 5.36 out of a theoretical maximum of 7.00.

Table 21: Score Prediction

	Mission 1	Mission 2	Mission 3	Ground Mission	Total
Cruise speed [ft/s]	53	63	66	—	—
Lap Number	3	3	7	—	—
Mission Time [s]	167	143	284	—	—
Dry weight [lb]	5.64	6.0	7.47	—	—
Payload weight [lb]	—	4.0	0.49	—	—
Projected Result	—	1.67 lb/min	12.1 lap	45 s	—
Best Result	—	10 lb/min	20 lap	30 s	—
Normalized Score	1	1.17	2.61	0.67	5.45

5.7. Drawing Package

The following drawing package includes a dimensional 3-view, subassemblies, and mission-specific payloads.











6. Manufacturing Plan

A wide variety of materials and associated manufacturing methods were evaluated for each critical component of the aircraft (including the motor mount, battery mount, wing mount, wings, empennage, etc.) to determine the optimal choice. This process was repeated for the mission systems, including the bottle adapter, pylon, XTV, and XTV attachment mechanism.

6.1. Investigated Processes, Selection Process, and Results

The team investigated a variety of manufacturing processes for each aircraft component after first determining that there was not a suitable off-the-shelf alternative. The manufacturing methods and processes for each component are detailed in the following sections.

6.1.1. Laser Cutting



Figure 32: Laser Cutter

Laser cutting is simple and quick, and can be used to manufacture large parts with high precision using computer-generated cutting paths. Its biggest limitations are the lack of versatility inherent to a Two-Dimensional (2D) manufacturing solution and the limited materials it can effectively penetrate.

6.1.2. Additive Manufacturing

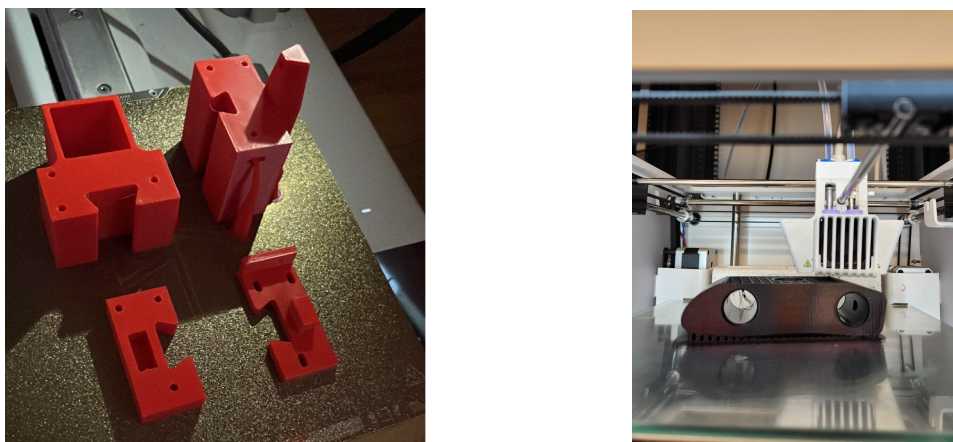


Figure 33: Aircraft Components Prototypes on FDM Printers



Figure 34: Prototype wing coupler prototyped using machining, FDM printing, and selective laser sintering (SLS) printing.

Additive manufacturing was another widely considered method, with the strengths and weaknesses of FDM, stereolithography (SLA), and SLS each evaluated. FDM parts are generally the lightest and benefit from the fastest manufacturing speed and largest maximum dimensions, with their greatest drawbacks being anisotropic properties and generally lower shear and tensile strengths. SLA printing was considered for its isotropic properties and high strength but was not used due to the increased weight that comes from parts being fully solid. SLS printing draws from the best of both of the previous methods with isotropic properties and a high strength-to-weight ratio, however, the parts it prints are limited in size by the machines available to the team.

6.1.3. Machining



Figure 35: Computer numerical control (CNC) lathe in use for manufacturing.

Machining is a highly precise subtractive manufacturing technique, primarily for metals. Materials are milled, turned, cut, drilled, or otherwise modified until they conform to the design geometry. Machining is extremely precise, though it is plagued by large setup times, material waste, and geometric limitations. The team thus limited machining to parts requiring high strength or precision. In the end the only machined parts in the final aircraft are the landing gear axles and control rods. The other parts machined proved to be far too heavy and did not require the strength of machined parts.

6.1.4. Composite Manufacturing

Composite manufacturing involves layering strands of a strong material such as carbon fibers, often in the form of woven sheets, and coating the layers in a resin that hardens and holds the individual fibers together. These materials are extremely strong but anisotropic. This process has limited geometries that can be achieved, cutting the fibers can be very toxic, and the strength of the material is directly dependent



on the process, unlike most materials. These factors combined with the fact that CU does not contain any approved dedicated locations to manufacture composites led the team to avoid this manufacturing process. Instead, off-the-shelf carbon fiber parts were purchased and modified, including the main structural rod, the wing spars, and the landing gear.

6.1.5. Component Security and Assembly

Various techniques were used to join components, such as glue, screws and nuts, velcro (also known as hook-and-loop tape), and nylon-reinforced adhesive tape.

Glue was chosen for lighter-load parts that would remain permanently attached. It was used primarily to attach components to the carbon fiber rods, including the electronics compartment and within the wings to connect the ribs to the wing spars. This was a cost-effective and efficient way to attach small and large components alike, with its only major downside being its permanence. A mix of hot glue and cyanoacrylate was used depending on the application. Hot glue was used in semi-permanent applications, or where there was a low contact area between parts. An example is securing the electronics compartment to the carbon fiber rod. Cyanoacrylate was used for permanent connections with high-contact areas, such as captive nuts.

Velcro was used for components that are frequently attached and removed, especially between mission configurations. Velcro was used in combination with adhesive tape to secure the electronics compartment where the receiver and associated components are stored. This allows for easy access to the components at any point during mission staging or the GM.

Captive nuts and corresponding screws were used for components that need to be easily attachable yet rigid. Choosing 4-40 screws as a standard size allows for efficient assembly with an electric screwdriver. There are some components that use other hardware sizes due to manufacturer specifications on off-the-shelf parts. Socket head cap screws in particular were chosen for their excellent strength and cam-out-resistant Allen heads. Nylon lock nuts were chosen as the preferred method for securing threaded hardware, except in instances that experienced rotational loads, where cotter pins were added. Loctite is also added to all permanently installed hardware prior to fastening, such as the hardware used to attach the motor to the motor mount.

Adhesive tape was used in certain cases that required hinged movement. Tape was used to attach the control surfaces to the corresponding wing/stabilizer, but is further secured with M2x0.4 hardware that prevents the tape from peeling off.

6.2. Detailed Manufacturing Processes

Each part of the aircraft was manufactured using one or more of the preceding manufacturing processes. Processes for the components were chosen based on manufacturing difficulty and expected loading.

6.2.1. Wings

The wings are designed with a standard MonoKote skin and carbon fiber and balsa skeleton. The structural core of each wing is a square carbon fiber rod, which provides rigidity and resists slipping or rotating due to its square profile. The wing rods insert into the 3D printed PLA wing mount to directly transfer the force of lift onto the aircraft and are held in place with two 4-40 bolts. To define the airfoil shape, a series of 0.125 in balsa ribs are spaced along the rod with a 3 in spacing. Where needed, these



standard balsa ribs can be substituted with 0.25 in ribs with servo cutouts. Additionally, a 0.0625 in thick balsa plate rests on the top side of the leading edge of the airfoil, providing further rigidity, and forming a defined leading edge, preventing the MonoKote from deforming in the most critical region. Along the trailing edge of the airfoil, a 0.25 in square balsa rod and an additional balsa strip are used to maintain consistent spacing and provide a second strong attachment point for the MonoKote. The control surfaces—a flaperon in this case—are attached to the trailing edge with a combination of adhesive tape, hardware, and rigid attachment via actuating rods.

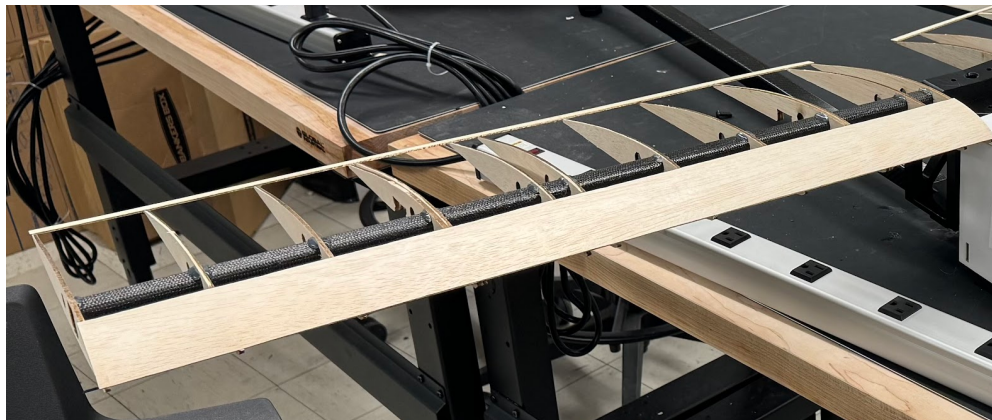


Figure 36: Prototype Wing Skeleton

MonoKote is a thin sheet of plastic that can be shrink-wrapped over a frame by applying heat, such as with a heat gun or iron. The team opted to use MonoKote to manufacture the wings of the aircraft, a departure from the team's previous competition aircrafts, which used foam board sheets for wings. This choice was made due to the extremely lightweight nature of MonoKote compared to foam board, as well as its greater ability to exactly replicate airfoil geometry. The relative fragility of MonoKote is mitigated by the ability to easily fix damage using patches of the same material, which may be done quickly and adds minimal weight.



Figure 37: Manufacturing the wing skin using MonoKote and a heating iron.



The manufacturing flow of the wings begins with the drilling of two holes in the carbon fiber rods that are used to secure the rods to the wing mount. The ribs are then slid into place with 3 in spaces between each rib and glued down. The flaperon servo is glued to the rib that is designed to accommodate it and its control horn is screwed into place. Once all the ribs are in place, the wing is wrapped in MonoKote and heating elements are used to shrink it into place. The installation of the flaperon begins with the outline and two holes being laser cut for the control horns. The control arm linkage is attached to the flaperon and the pair are taped into place. The wings are then slid into the crossbar mount and the 4-40 retaining hardware is installed.

6.2.2. Fuselage

The team opted to create an aircraft devoid of a central fuselage. The aircraft instead features a variety of 3D printed components attached to the central rod serving many of the same functions as a traditional fuselage. This includes the battery mount, wing mount, electronics compartment, motor mount, empennage adapter, and payload assembly. The electronics compartment, which houses the receiver, ESC, fuse, and safety switch, is a 3D printed part but features a unique hinge made out of unprocessed PLA filament. The filament is used as the axle of the hinge and is melted into place to prevent it from falling out of the hole. In summary, the parts that would traditionally be viewed as a fuselage are by and large 3D printed, screwed together, slid onto the central structural rod, and glued into place. This is excluding the wings which are clamped onto the rod to allow for a higher degree of mobility to maintain the same relative CG for all 3 missions.

6.2.3. Empennage

The empennage was constructed out of laser-cut foam, with the stabilizers press-fit and superglued to one another. Adhesive tape was used to hold the laser-cut foam control surfaces onto the main stabilizer surfaces, providing both strength and freedom of movement. The tape holding the stabilizers is compressed between two sheets of foam board to stop it from peeling off. Two small square carbon fiber rods were slotted through the horizontal stabilizer to provide structural rigidity and two more act as trusses between the horizontal stabilizer and vertical stabilizer. The entire empennage assembly is connected to the central rod with a 3D printed part. This part is hot glued to the horizontal stabilizers and has a hole for a bolt that goes completely through the rod.



Figure 38: Empennage

6.2.4. Landing Gear

Both the front landing gear and tail wheel are made from off-the-shelf components. The front gear is made from carbon fiber composite and is mounted onto the structural rod with a PLA 3D print. The printed part contains captive nuts that secure bolts which go through the landing gear. The tail wheel is an off-the-shelf caster wheel mounted onto the structural rod with a PLA 3D print and held in place with a cotter pin and cyanoacrylate.

6.2.5. Payload System

The payload system is split into two parts, the fuel tank system and the XTV system. The fuel tank system is entirely manufactured with FDM printing, except for off-the-shelf springs and hardware. These parts are



fastened together in 3 sub-sections: fuel tank, pylon, and pylon mount. For the fuel tank, the bottle adapter is super glued to the fuel tank, and the tank is filled with metal and rice to the desired weight. The pylon assembly requires the fastening of several screws and the insertion of a spring. The pylon mount requires the same assembly steps but is also hot glued to the central structural rod once assembled.

While the XTV is based on an off-the-shelf model, it features 3D printed parts to accommodate the modifications made by the team. To build the XTV, the motor is removed and the wires connecting it are cut. The front section of the foam Top Race RC Plane is then removed using a handheld hot wire cutter. The 3D printed compartment is super glued to the front of the model using foam-safe super glue. The compartment has a hinging door that uses the previously explained filament hinge. Velcro and adhesive tape are used to seal the door. The final stage of assembly involves installing all the electronics to the compartment and attaching the drop mechanism adapter and Hall Effect sensor to the top of the XTV.

6.2.6. General Assembly

Once all of the individual subsystems have been manufactured, the aircraft assembly begins. Due to the distributed systems, each individual system can be manufactured in parallel allowing for a shorter manufacturing period. With all the systems complete the remaining assembly involves sliding all of the different components onto the rod and checking weight and balance predictions to ensure the proper CG relative to the center of lift. The adjustable nature of the wings means that once all components are in position, the location of the wings is marked for each mission, and all other components are glued to the rods with hot glue to prevent them from sliding. This process allows for easy assembly and disassembly of the aircraft for transport to and from the testing location and competition.

6.3. Manufacturing Milestone Chart

The spring semester schedule involved six weeks of assembly, followed by flight tests, manufacturing of spare components, and last-minute revisions in March and April, should the need arise. This schedule is more ambitious than previous years, giving the team more breathing room to test and prepare for competition. This is the manufacturing timeline for the final competition-ready aircraft. This excludes prototypes that have previously been developed and those that are being developed concurrently, as their schedules are far more flexible and constantly evolving.

Manufacturing Milestones		February				March					April	
		3	10	17	24	3	10	17	24	31		
Kitting	LaserCutting									Key		
	3D Printing									Planned		
Wings	Wing Jig Assembly									Actual		
	MonoKote Application									///		
	Control Surfaces											
	Component Assembly											
Landing Gear	Tail Gear											
	Main Landing Gear											
Empennage	Vertical Stabilizer											
	Horizontal Stabilizer											
Others	X-1 Test Vehicle										DBF FLY-OFF	
	Electrical Integration											
	Redundancies											
	Flight Tests											

Figure 39: Manufacturing Milestones for AIAA DBF 2024-2025



7. Testing Plan

A series of tests were done on the aircraft and its components to validate their design and performance. The data gained from these tests has guided the ongoing development of the final aircraft.

7.1. Test Objectives and Schedule

The test schedule presented in Table 22 outlines the planned tests for each subsystem of the aircraft.

Table 22: Testing Schedule

	Test	Date	Method	Objective
Propulsion	Static Thrust	02/10/25	Fix the system to a thrust bench, and run the motor until the batteries are fully discharged. Monitor metrics including thrust, current draw, and battery voltage.	Determine motor-generated thrust, power, RPM, and current draw for various propeller and motor combinations to optimize propulsion efficiency.
	Batteries & Fuse	02/10/25		Estimate the battery discharge rate and assess current draw to ensure reliable power delivery.
Ground	Wing Tip	02/15/25	Balance the aircraft on its wingtips with maximum mission weight and verify structural integrity.	Ensure the wings can carry the full weight of aircraft (including payload) without plastic deformation.
	Signal Range	02/18/25	Incrementally move the controller away from aircraft and test the response of the electrical components.	Find maximum operational distance for controller and aircraft.
	Steering System	02/18/25	Taxi the aircraft on the ground.	Test the maneuverability of the aircraft on ground.
	Assembly	03/25/25	Simulate Ground Mission; a single student will assemble the test program aircraft while timed.	Determine the time required to assemble the aircraft. Identify possible improvements.
Component	Structural	01/25/25	Apply expected loads while observing deformation and stress concentrations in SOLIDWORKS.	Ensure structures can withstand expected loads during takeoff, flight, and landing.
	Wind Tunnel	02/04/25	Place a scale model of the wing into a wind tunnel.	Determine aerodynamic properties of the wing.
	Destructive Testing	02/11/25	Bend components with a force equivalent to that experienced in FEA and ensure they do not fail.	Ensure all manufactured parts are structurally sound.
	Motor Mount	02/15/25	Attach weights to the motor mount equivalent to maximum thrust.	Ensure the airframe can withstand the maximum thrust generated by the motor.
	Landing Gear	02/15/25	Drop the weighted aircraft from 3 feet.	Test the impact resistance of the landing gear.
	Component Security	02/25/25	Subject the fully loaded aircraft to higher g-forces than it will experience in flight and landing.	Ensure internal and external components are secured in place, e.g., batteries, payload, receiver, ESCs.
	XTV Release Mechanism	03/11/25	Release the XTV with electrical components from the aircraft onto padding.	Ensure the release mechanism performs as expected and the flashing lights of the XTV activate and remain operational.
Flight	XTV Flight	03/15/25	Drop the XTV from a previously designed and tested airframe.	Evaluate mission efficacy for the XTV.
	Flight Test #1	02/09/25	Perform the delivery flight with the no payload installed.	Simulate Mission 1: Delivery Flight. Test basic flight capabilities, controllability, and stability of aircraft.
	Flight Test #2	03/22/25	Fly the aircraft with the XTV and fuel tanks.	Simulate Mission 2: Captive Carry Flight. Ensure desired mission performance and identify possible improvements.
	Flight Test #3	03/22/25	Fly the aircraft with fuel tanks and release the XTV.	Simulate Mission 3: Launch Flight. Ensure desired mission performance and identify possible improvements.



7.1.1. Propulsion Testing

The propulsion testing aimed to confirm that the aircraft's theoretical propulsion characteristics aligned with the experimental values. The aircraft's maximum velocity, acceleration, and takeoff time are directly influenced by the total thrust produced by the propeller. To quantify this thrust, the test apparatus shown in Fig. 40 was developed.

The propeller is mounted on a rigid aluminum frame that pivots about a hinge, allowing it to rotate in response to the thrust. A horizontal extension arm presses against a scale, which provides a force measurement. However, since the thrust force and the scale force act at different distances from the pivot, the scale reading does not directly represent the actual thrust. Instead, the ratio of the lever arm lengths was used to calculate the true thrust force.

Before testing, the scale was zeroed and the motor speed was slowly increased while checking for vibrations, misalignment, or interference with surrounding components. Once stable operation was confirmed, the throttle was steadily increased to full power, recording the scale reading at each step. Using the measured lever arm ratio, a maximum thrust of 13.01 lbf at full throttle was determined.

Additionally, to verify battery performance met manufacturer specifications, the team performed a battery drain test on the same apparatus as the static thrust test, instead with a battery voltage monitoring device installed. Two tests were performed, one with the thrust level maintained at 100 percent—which could be precisely determined by accessing the thrust channel output on the transmitter—and one test where the thrust was maintained at 50 percent. The data was then processed and results were subsequently analyzed.

7.1.2. Ground Testing

7.1.2.1. Wing Tip Testing

As a preliminary wing tip load test, the aircraft was supported from the wingtips and loaded at the CG to validate that the wing mount would exceed the minimum required strength to maintain structural integrity during flight.

7.1.2.2. Signal Range Testing

To perform signal range testing, an individual holding the transmitter remained stationary while continuously moving a servo motor via the transmitter. Another individual walked away from the transmitter, holding the receiver, battery, and servo motor to verify connectivity. The location at which the servo was observed to no longer continuously respond to the inputs from the transmitter was recorded, and the distance was extrapolated through the use of digital map software.

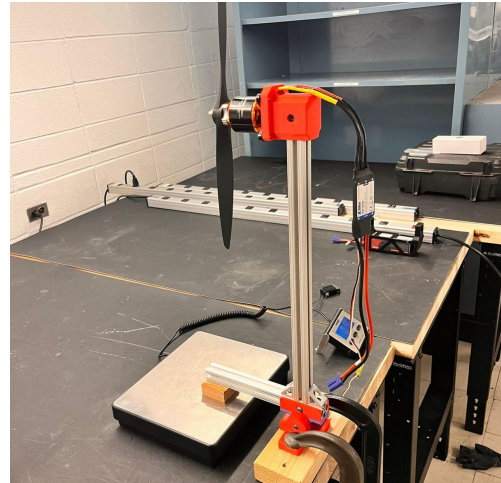


Figure 40: Motor and Propeller Testing Stand (battery not shown)



7.1.2.3. Steering System Testing

This test was performed by taxiing the aircraft in various directions and assessing its ability to turn, maintain a straight path, and respond smoothly to steering inputs. The test verified that the aircraft can navigate taxiways and takeoff positions effectively.

7.1.3. Component Testing

7.1.3.1. Structural Testing

Structural testing was conducted using SOLIDWORKS simulation tools to apply expected aerodynamic, inertial, and landing loads to the aircraft's structure. FEA was conducted to observe deformation, stress distribution, and potential failure points in key structural components, the wing spars, landing gear, and mounting points. As shown in section 5.2 the results were analyzed to determine if reinforcements or design modifications were necessary.

7.1.3.2. Wind Tunnel Testing

Wind tunnel tests were conducted to verify the aerodynamic behavior of the aircraft and compare theoretical predictions with real-world performance. These tests were performed in the experimental wind tunnel at the CU Mechanical Engineering Teaching Laboratory. A 1:1 scale model of the wing was fabricated and placed in the wind tunnel, as shown in Fig. 41. The wind tunnel tested a range of airspeeds, while a dynamometer measured the lift and drag generated. The collected data was then used to extrapolate and predict the lift and drag for the full wingspan of the aircraft.

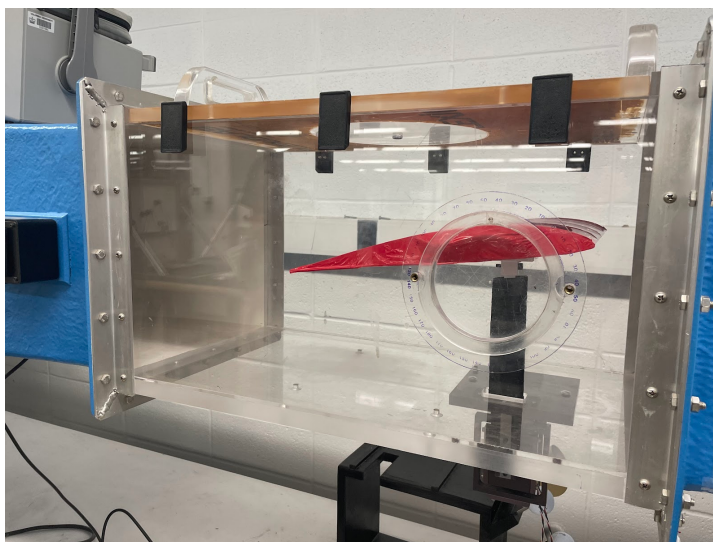


Figure 41: Prototype wing section mounted into the testing chamber of the wind tunnel.

7.1.3.5. Landing Gear Testing

To verify the landing gear could sustain the impact upon landing, drop testing was performed at maximum (M2) weight from a height of 3 ft. The landing gear showed no signs of failure, and the structural integrity



of the landing gear and other components that could be subjected to higher forces during landing was confirmed through disassembly and visual inspection.

7.1.3.6. Test Vehicle Release Mechanism Testing

The XTV release mechanism test involved releasing the XTV from the main aircraft onto some padding to ensure release mechanism reliability. The test will also verify the XTV electronics by the activation and continuous operation of the flashing lights and guidance systems upon release.

7.1.4. Flight Testing

Flight tests are a critical step in validating the aircraft's predicted performance. Each test was conducted to simulate different mission conditions to verify theoretical designs and models. The performance of all subsystems will be monitored throughout testing, with iterative improvements made as needed to address any performance issues. Flight of a prototype aircraft to evaluate proposed landing gear, control surfaces, and empennage for *Carrier Pigeon* was completed early in the spring semester. The flight test for the final 2025 DBF aircraft is scheduled for mid-March, with additional tests proceeding up until the competition.

7.1.4.1. Test Vehicle Flight Testing

The XTV will be released from a previously validated airframe to assess its flight characteristics and autonomous performance. Testing will evaluate stability, control, and the ability to execute the required flight path, including a 180° turn and landing in the designated area. Additionally, air and weather conditions—such as air pressure and temperature—will be recorded. Success criteria include smooth separation, controlled descent, and mission completion within the required time frame.

7.1.4.2. M1 Flight Testing

The aircraft will undergo its initial flight to assess basic flight performance, controllability, and stability under normal conditions. The test will simulate M1, where the aircraft operates without external payloads or modifications. Key evaluation points include takeoff, sustained flight, maneuverability, and a controlled landing to confirm airworthiness.

7.1.4.3. M2 Flight Testing

The aircraft will be tested with mounted fuel tanks and the XTV to simulate M2, and evaluate its performance under payload conditions. This test will assess takeoff capability and maneuverability with added weight, the ability to maintain controlled flight throughout the mission, and the execution of a safe landing.

7.1.4.4. M3 Flight Testing

The aircraft will carry and deploy the XTV mid-flight to simulate M3. The test will focus on takeoff and stable flight while carrying the payload, as well as proper execution of the release mechanism and lights.

7.2. Checklists

Flight tests require detailed checklists to ensure that there is no malfunction during flight due to human error. It ensures that both the aircraft and the humans around it are safe, barring any extreme external factors. Table 23 shows the checklist used by CU AIAA.



Table 23: Flight Checklist

PRE-FLIGHT		PRE-TAKEOFF	
Aircraft Assembly		Propulsion battery Installed	
	Fasteners & hardware Secure		Receiver battery Installed
	Cables & connectors Secure		Transmitter On
	Landing gear Secure		Throttle safety On
	Servos, linkages & horns Secure		Electronics On
	Control surfaces Secure		Control surfaces Functioning
	Wings Secure		Arming plug Armed
	Payload (if required) Secure		Throttle safety Off
Electronics & Propulsion		Propulsion Functioning	
	Propulsion battery Charged, Secure	POST-LANDING	
	Electronics battery Charged, Secure		Throttle safety On
	ESC Secure		Arming plug Disarmed
	Receiver Secure		Electronics Off
	Controls Trimmed, Centered		Propulsion battery Unplug
	Failsafe Check		Receiver battery Unplug

The team also used checklists for propulsion and aerodynamics tests to ensure that proper procedures were followed before and after each test. These checklists are shown in Table 24.

Table 24: Test Checklist

PROPULSION		AERODYNAMICS	
Before Test		Before Test	
	Test rig Secure		Test rig Secure
	Throttle safety On		Wing Secure
	Propulsion battery Charged, Secure		Sensors Calibrated
	ESC Secure		AoA Fixed
	Receiver Secure		Software On
	Propeller Secure		Test area Clear
	Camera On		Power On
	Test area Clear	After Test	
	Throttle safety Off		Power Off
After Test			Data Saved
	Throttle safety On		Wing Remove
	Camera Off		
	Propulsion Battery Unplug		



8. Performance Results

This section details the results of the aforementioned performance tests. The data acquired in these tests were compared to the predicted performances to provide insight into potential improvements to the design of the aircraft.

8.1. Ground Test Results

This section constitutes all tests that were done in the usual laboratory space of CU AIAA. Future sections detail tests done at the airfield.

8.1.1. Structural Test Results

8.1.1.1 Wing Tip Testing

The results from the wing tip test proved that revisions were necessary for certain structural components. Fig. 42 shows the aircraft balanced in the wingtip test. Originally, this test was done on a previous iteration of the wing mount. 13.38 lb of weight were applied to the wing mount through means of a backpack filled with mass. When the wing tip testing was performed, the wing mount failed, the maximum force exceeding the material limits. The wing mount was then redesigned to be sturdier at the region where the wings interface with the wing mount. To verify that the changes were satisfactory, an FEA was performed, visible in Fig. 20. The factor of safety was 3.94 for this improved version. This improvement was then tested and confirmed, depicted in Fig. 43.



Figure 42: Aircraft Balanced from Quarter Chord

Fig. 43 shows the vertical load test in progress. The load in the bag translated into an effective load of 65 lbf when the specific geometry of the reaction forces acting at the wingtips were considered.



Figure 43: Wingtip load test. An additional load of 13 lb was added on top of the full M2 configuration—the heaviest configuration. Note that the load is above the ground.

8.1.1.2 Signal Range Testing

The signal range test quantified the approximate range of the transmitter. Since the team performed this test in an environment with tall buildings, signal interference was expected, which would limit the actual range. To conduct the test, a team member holding the receiver walked in a straight line from the position of the transmitter until the signal was lost. The transmitter lost signal at a range of 4,329 ft, which is plotted using mapping software in Fig. 44.

8.1.1.3 Steering System Testing

The taxi test demonstrated that the aircraft could maneuver with precision, maintaining stability and control. The aircraft successfully executed smooth turns, held a consistent straight path without unintended deviations, and responded promptly to steering inputs. These results confirm that the landing gear and ground handling system are well-optimized for reliable taxiing, ensuring the aircraft can navigate taxiways and reach takeoff positions efficiently.

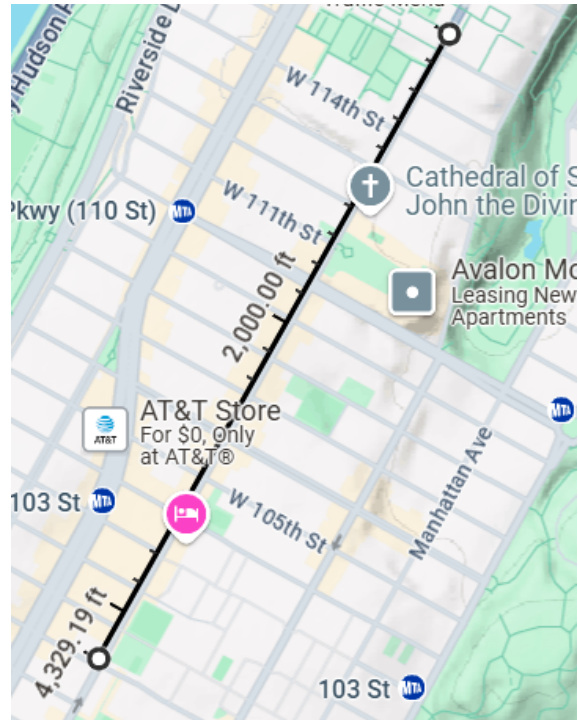


Figure 44: Signal Range Measurement

8.1.2. Aerodynamic Test Results

Fig. 45 displays the lift generated by the S7055 airfoil section at a range of airspeeds. The lift is renormalized to correspond to the wingspan. At the wind tunnel's maximum airspeed of 55 ft/s, the



estimated lift fluctuates around 28 lb. This is slightly more than the theoretical lift of 26 lbs, as calculated using flow analysis. Since the span of the test airfoil was smaller than the chord length of the airfoil, vortices caused by the ends of the test piece may have greatly affected the lift and likely contributed to the instability. Manufacturing imperfections, amplified by the small size, also could have contributed. More testing with more AoAs will provide further insight on the performance of the aircraft in flight, in addition to full scale flight testing.

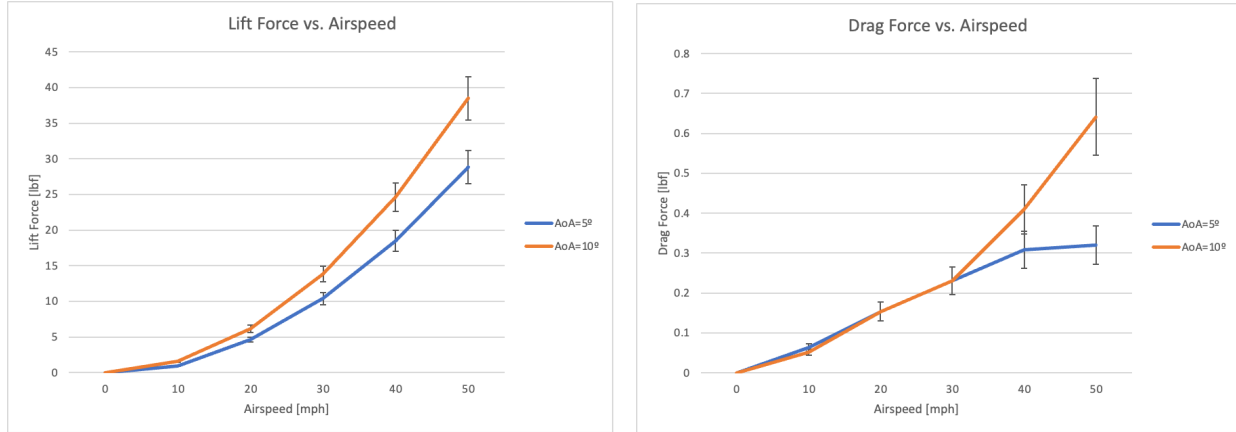


Figure 45: Lift and drag generated by S7055 airfoil vs airspeed, renormalized to correspond with full wingspan.

8.1.3. Avionics and Propulsion Test Results

The team conducted two propulsion tests to verify the manufacturer's stated thrust values and stated capacity. Fig. 46 shows the lowest LiPo cell voltage over time. This test yields a worst case scenario of approximately 11 minutes of airtime when the motor is at 50% throttle. The test verified that the battery could sustain propulsion for the full expected duration of the flight. Fig. 47 shows the thrust vs throttle curve of the motor. The maximum thrust recorded was 13.01 lbs which is inline with the manufacturer's stated 9 to 14.5 lb rating.

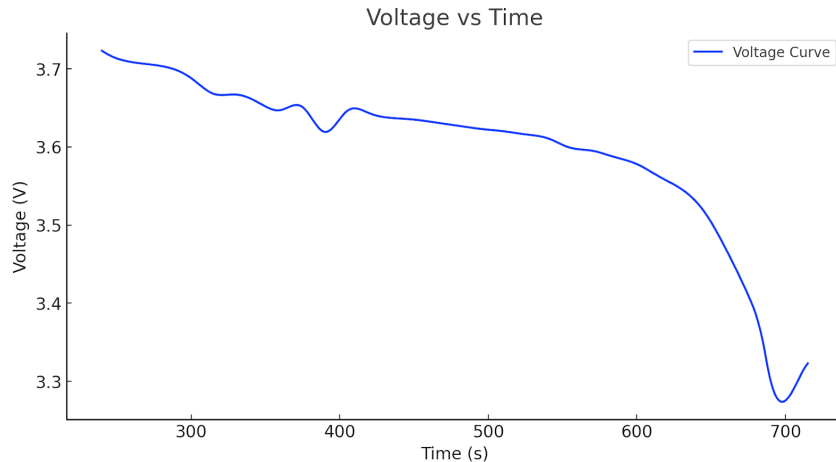


Figure 46: Lowest LiPo cell voltage over time when run at 50% throttle.

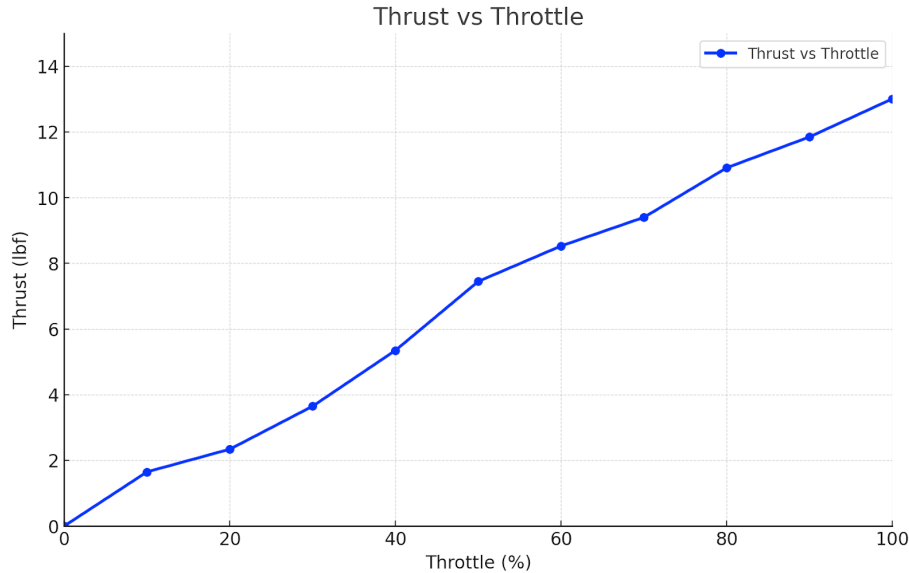


Figure 47: Throttle vs Thrust curve

8.2. Flight Test Results

The prototype test flight was conducted on Feb 9, 2025, with two primary goals: to verify that the aircraft was indeed airworthy, and if possible, to simulate M1. Atmospheric conditions that day were fair for testing with calm winds, an atmospheric pressure of 30 inHg, and a temperature of 34° F.

The prototype aircraft was set up without external payloads, matching the specification requirements for M1. The first flight was conducted to ensure stable flight was possible. After taking off, the pilot adjusted for trim and got a feel for the flyability of the plane by practicing basic maneuvers such as banking and climbing. After landing and switching to a fully charged battery, the pilot simulated a run of M1, following the course as described in Section 3.1.1.

Despite the fair weather conditions, the time to complete 3 laps was 4 min 39 s, which was slower than the predicted M1 performance. The pilot mentioned the roll control was suboptimal. To address this issue, the Aerodynamics Team increased the flaperons' width by 10 percent to their current size.

8.3. Differences to Predictions and Improvements

Overall, physical testing performed reasonably close to expectations given by simulation and testing predictions. For example, the airfoil's wind tunnel lift and drag were within 10% of the simulated tests. Major differences included underpowered yaw and pitch control. Improvements include resizing the flaperons, replacing the battery, adjusting the landing gear design to prevent side-to-side movement, and minimizing drag to reduce motor power required to fly at cruising speed.



Figure 48: Aerial View from Prototype Aircraft

9. Bibliography

- [1] *2024-2025 Design, Build, Fly Rules*. (n.d.). AIAA.
<https://www.aiaa.org/docs/default-source/uploadedfiles/aiaadb/resources/dbf-rules-2025.pdf>
- [2] *Airfoil Tools*. (n.d.). <https://airfoiltools.com>
- [3] *National Weather Service*. (2025). <https://weather.gov>
- [4] Raymer, D. P. (2006). *Aircraft design: A conceptual approach* (4th ed.). American Institute of Aeronautics and Astronautics.
- [5] MIL-F-8785B: Flying Qualities of Piloted Aircraft. (1969). Department of Defense.
- [6] *2024-2025 Design, Build, Fly Question and Answer Number 4* AIAA.
https://www.aiaa.org/docs/default-source/uploadedfiles/aiaadb/resources/2024-25-dbf-q-a-4.pdf?sfvr_sn=94707da2_2
- [7] Travieso-Rodriguez, J. A., Jerez-Mesa, R., Llumà, J., Traver-Ramos, O., Gomez-Gras, G., & Roa Rovira, J. J. (2019). Mechanical Properties of 3D-Printing Polylactic Acid Parts subjected to Bending Stress and Fatigue Testing. *Materials* (Basel, Switzerland), 12(23), 3859.
<https://doi.org/10.3390/ma12233859>
- [8] *Bambu Filament Technical Data Sheet V3.0*. (n.d.). Bambu Lab.
<https://store.bblcdn.com/s5/default/6cc09734a85147e9a6d3307ffd808498.pdf>